Technical Note: Evaluation of simultaneous measurements of mesospheric OH, HO_2, and O_3 under photochemical equilibrium assumption: Statistical approach

Mikhail Yu. Kulikov[1], Anton A. Nechaev[1], Mikhail V. Belikovich[1], Tatiana S. Ermakova[1], and Alexander M. Feigin[1]

[1]Institute of Applied Physics of the Russian Academy of Sciences, 46 Ulyanov Str., 603950 Nizhny Novgorod, Russia

Correspondence to: Mikhail Yu. Kulikov (mikhail_kulikov@mail.ru)

Abstract

The Technical Note presents a statistical approach to evaluating simultaneous measurements of several atmospheric components under the assumption of photochemical equilibrium. We consider simultaneous measurements of OH, HO_2, and O_3 at the altitudes of the mesosphere as a specific example and their daytime photochemical equilibrium as an evaluating relationship. A simplified algebraic equation relating local concentrations of these components in the 50-100 km altitude range has been derived. The parameters of the equation are temperature, neutral density, local zenith angle, and the rates of 8 reactions. We have performed a one-year simulation of the mesosphere and lower thermosphere using a 3D chemical-transport model. The simulation shows that the discrepancy between the calculated evolution of the components and the equilibrium value given by the equation does not exceed 3-4% in the full range of altitudes independent of season or latitude. We have developed the technique of statistic Bayesian evaluation of simultaneous measurements of OH, HO_2 and O_3 based on the equilibrium equation taking into account the measurement error. The first results of application of the technique to MLS/Aura data are presented in this Technical Note. It has been found that the satellite data of HO_2 distribution regularly demonstrates essentially lower altitudes of mesospheric maximum of this component. This has also been confirmed by model HO_2 distributions and comparison with offline retrieval of HO_2 from the daily zonal means MLS radiance.

1. Introduction

A prominent feature of the atmospheric photochemical systems is the presence of a large number of chemical components with short lifetime and concentrations close to stable photochemical equilibrium at every instant. The condition of balance between their sources and sinks is described by a system of algebraic equations. This system can be used to determine characteristics of hard to measure atmospheric species through other measurable components, validate results of remote or *in situ* measurements, estimate reaction rates usually known with significant uncertainty, and to understand processes and chemical reactions that influence variability of the most important atmospheric components, e.g. ozone, in the geographical region of interest.

This approach has found wide application:

(1) in 3D chemical transport models that include a large set of physical and chemical processes with a broad spectrum of spatio-temporal scales. In particular, the chemical family concept is widely used for simulating gas phase photochemistry of the lower and middle atmosphere (e.g., Douglass et al., 1989; Kaye and Rood, 1989; Rasch et al., 1995), when transport is taken into account only for the concentration of a chemical family, while relative concentrations of the constituent fast components are calculated from the instantaneous stable equilibrium condition. Complemented with the Henry law (e.g., Djouad et al., 2003; Tulet et al., 2006) in multiphase models, this approach markedly saves calculation time and increases the overall stability of the numerical scheme. Moreover, the use of the photochemical equilibrium condition to simulate fast components dynamics reduces the phase space dimension of box models significantly (e.g., Kulikov and Feigin, 2014), allowing a comprehensive analysis of nontrivial nonlinear dynamic properties of various atmospheric photochemical systems (e.g., Feigin and Konovalov, 1996; Feigin et al., 1998; Konovalov et al., 1999; Konovalov and Feigin, 2000; Kulikov et al., 2012).

(2) in investigations of the chemistry of the surface layer and free troposphere in different regions (over megalopolises, in rural areas, in the mountains, over the seas) based on measurements of nitrogen species, peroxy radicals, ozone, aerosols, and other components aimed at understanding processes impacting the surface ozone formation and air quality. The equilibrium condition is most frequently used for nitrogen species. For example, Chameides (1975) proposed a model for determining the vertical distribution of odd nitrogen, in which the HNO_3 profile could be

63 deployed to retrieve profiles of five other components (NO, NO_2, NO_3, N_2O_5, and HNO_2) from their
64 photochemical equilibrium condition. In the paper by Stedman et al. (1975) the equation for NO_2
65 equilibrium that accounted only for the main source and sink of this component was applied to
66 determine the photodissociation constant $J(NO_2)$. A more accurate equation for the NO_2 equilibrium
67 was used by Crawford et al. (1996) and Kondo et al. (1996) to determine the NO_2/NO partitioning
68 and NO_x, allowing, in particular, investigating the spatial distribution of NO_x/NO_y over the Pacific.
69 Night-time equilibrium in the NO_2-NO_3-N_2O_5 system is used to determine surface layer N_2O_5
70 concentration, equilibrium constant of this system, equilibrium partitioning between NO_3 and N_2O_5,
71 and loss coefficients of NO_3, N_2O_5 and NO_x (Martinez et al., 2000; Brown et al., 2003; Crowley et
72 al., 2010; McLaren et al., 2010; Benton et al., 2010; Sobanski et al., 2016).
73 Platt et al. (1979) used the CH_2O photochemical equilibrium condition to analyse results of
74 simultaneous measurement of CH_2O, O_3 and NO_2 and to identify mechanisms of CH_2O formation
75 over rural areas and in maritime air. In the papers by Ko et al. (2003), Cantrell et al. (2003),
76 Penkett et al. (1997), Penkett et al. (1998) algebraic expressions derived from equilibrium
77 conditions for H_2O_2, peroxy radicals and nitrogen species were used to determine equilibrium
78 values of peroxide concentration, total peroxy radical level, and NO/NO_2 ratio, and to diagnose the
79 ozone production and loss levels in clean or polluted troposphere.
80 (3) in stratospheric chemistry studies, including determination of a critical parameter in
81 catalytic cycles of ozone destruction in the polar stratosphere. In particular, the equilibrium
82 condition for ClO and Cl_2O_2 along with the measurement data of daytime and night-time
83 concentrations of these components in the polar stratosphere are used to evaluate the temperature
84 dependence of the ClO concentration, reaction constants determining the
85 $ClO + ClO + M \leftrightarrow Cl_2O_2 + M$ equilibrium, and the photolysis rate of Cl_2O_2 (Ghosh et al., 1997;
86 Avallone et al., 2001, Solomon et al., 2002; Stimpfle et al., 2004; von Hobe et al., 2005; Berthet et
87 al., 2005; Butz et al., 2007; von Hobe et al., 2007; Kremser et al., 2011; Sumińska-Ebersoldt et al.,
88 2012; Wetzel et al., 2012).
89 Pyle et al. (1983) proposed a method for derivation of the OH concentration from satellite
90 infrared measurements of NO_2 and HNO_3 using a simple algebraic relation following from the
91 equilibrium condition for HNO_3. Algorithms for retrieving distributions of OH and HO2 from the
92 satellite measurement data of O_3, NO_2, H_2O, HNO_3 by LIMS/Nimbus 7 and UARS with the help of
93 algebraic models following from the photochemical equilibrium of O_x, HO_x and HNO_3 components

were proposed by Pyle and Zavody (1985), Pickett and Peterson (1996). It is also worthy of note that similar models are widely used for calculating concentrations of components with a short lifetime (e.g. $O(^1D)$ and OH) and subsequent evaluating vertical distributions of eddy diffusivity from measurements of trace gas concentration profiles (see, e.g., Massie and Hunten, 1981).

Kondo et al. (1988) made use of the photochemical equilibrium between NO and NO_2 for understanding diurnal variations of NO concentration measured during aircraft flights. In the paper by Webster et al. (1990) simultaneous *in situ* balloon-borne measurements of NO, NO_2, HNO_3, O_3 and N_2O and the photochemical equilibrium condition for various nitrogen components were used to determine OH, N_2O_5 and NO_y concentrations. A similar approach was employed by Kawa et al. (1990), who obtained NO_2, N_2O_5, $ClNO_3$, HNO_3 and OH concentrations from aircraft measurements of NO, ClO and O_3 concentrations. Hauchecorne et al. (2010) found that NO_3 concentration measured by GOMOS/ENVISAT positively correlates with temperature at altitudes up to 45 km in the region where NO_3 is in chemical equilibrium with O_3. Funke et al. (2005) used NO and NO_2 stable-state photochemistry to verify correctness of the new approach of retrieving distributions of those component from MIPAS/ENVISAT measurement data. Marchland et al. (2007) proposed a method to retrieve the temperature distribution in the stratosphere between 30 km and 40 km from O_3 and NO_3 measurements by GOMOS with the help of a simple equation derived from the night-time NO_3 chemical equilibrium.

(4) in investigations of the chemistry of O_x–HO_x components and atmospheric glows in the mesosphere and MLT area. In particular, Kulikov et al. (2006, 2009) proposed algorithms for the simultaneous retrieval of O, H, HO_2 and H_2O from joint OH and O_3 satellite measurement, in which the assumption of photochemical equilibrium of O_3, OH, and HO_2 was utilized. For several decades the assumption of the photochemical equilibrium of ozone (PEO) was widely used to determine distributions of atomic oxygen and atomic hydrogen at altitudes of the MLT via satellite and rocket measurement of ozone concentration and airglow emissions (e.g., Evans and Llewellyn, 1973; Good, 1976; Pendleton et al., 1983; McDade et al., 1985; McDade and Llewellyn, 1988; Evans et al., 1988; Thomas, 1990; Llewellyn et al., 1993; Llewellyn and McDade, 1996; Mlynczak et al., 2007, 2013a, 2013b, 2014; Smith et al., 2010; Siskind et al., 2008, 2015). Russell and Lowe (2003) applied PEO to infer the seasonal and global climatology of atomic oxygen using WINDII/UARS. PEO was deployed to investigate hydroxyl emission mechanisms, morphology, and variability in the upper mesosphere – lower thermosphere region (Marsh et al., 2006; Xu et al., 2010, 2012;

Kowalewski et al., 2014). Mlynczak and Solomon (1991, 1993) and Mlynczak et al. (2013b) used the equilibrium assumption to derive exothermic chemical heat. The PEO assumption employed for studying the mesospheric OH* layer response to gravity waves (Swenson and Gardner, 1998). In ultimately theoretical works, e.g. Grygalashvyly et al. (2014), Grygalashvyly (2015), PEO was used to derive the dependence of excited hydroxyl layer concentration and altitude on atomic oxygen and temperature. In the paper by Sonnemann et al. (2015) it was used to analyze annual variations of OH* layer. Moreover, PEO is frequently applied implicitly, when authors are equating the night-time loss of ozone in the reaction with atomic hydrogen and production of ozone by a 3-body reaction of molecular and atomic oxygen (e.g., Nikoukar et al., 2007).

In the present Technical note we demonstrate how the photochemical equilibrium condition of several atmospheric components may be employed to statistically validate data of their simultaneous measurements, particularly in the case when measurement error is large.

We consider the simultaneous photochemical daytime equilibrium of OH, HO_2, and O_3 at the altitudes of the mesosphere. We have derived a simplified algebraic equation

$$F(OH, HO_2, O_3) = 1,$$

describing the relationship between local concentrations of the components at the altitudes of 50–100 km. The only parameters of the equation are temperature, neutral density, local zenith angle, and constants of 8 reactions. One-year simulation of the mesosphere and lower thermosphere based on a 3D chemical-transport model shows that the discrepancy between the calculated evolution of the components and the equilibrium value given by the equation does not exceed 3–4 % in the full range of altitudes independent of season or latitude.

We have developed a technique of statistical Bayesian evaluation of simultaneous measurement of OH, HO_2 and O_3 based on the mentioned equilibrium equation taking into account the measurement error. The first results of its application to MLS/Aura data (Wang et al., 2015a,b; Schwartz et al., 2015) are presented. It is found that the satellite data of HO_2 distribution regularly demonstrates essentially lower altitudes of this component's mesospheric maximum. These results confirm the ones obtained via the offline retrieval of HO_2 from the MLS primary data (Millán et al., 2015).

The Technical Note is structured as follows. A 3D chemical transport model is briefly described in Sect. 2. In Sect. 3 a simplified algebraic relationship between the equilibrium concentrations of OH, HO_2 and O_3 is derived and verified by 3D simulations. Section 4 presents the

156 method of statistical evaluation of simultaneous data of OH, HO_2 and O_3. The results of applying
157 the method to MLS/Aura data are presented in Sect. 5. The last Section contains discussion of the
158 results followed by concluding remarks.
159
160 **2. Model and calculations**
161
162 For our calculations we used the global 3D chemical transport model (CTM) of the middle
163 atmosphere developed by the Leibniz Institute of Atmospheric Physics (IAP) (e.g., Sonnemann et
164 al., 1998). It was designed particularly for investigation of the spatio-temporal structure of
165 phenomena in the MLT region and specifically in the extended mesopause region. The grid-point
166 model extends from the ground up to the middle thermosphere (0–150 km; 118 pressure-height
167 levels). The horizontal resolution amounts to 5.625° latitudinally and 5.625° longitudinally. The
168 chemical module described in numerous papers (e.g., Sonnemann et al., 1998; Körner and
169 Sonnemann, 2001; Grygalashvyly et al., 2009, 2011, 2012) consists of 19 constituents, 49
170 chemical reactions, and 14 photo-dissociation reactions (see Table 1). The reaction rates used in
171 the model are taken from Burkholder et al. (2015). The temperature-dependent reaction rates are
172 calculated on-line, thus, they are sensitive to small temperature fluctuations. We make use of the
173 pre-calculated dissociation rates (Kremp et al., 1999).
174 The evolution of the components of HO_x (H, OH, HO_2, H_2O_2) and NO_x (N, NO, NO_2, NO_3)
175 families is calculated using the chemical family concept proposed by Shimazaki (Shimazaki, 1985).
176 This is done because of the presence of short-lived components among these families, with
177 lifetimes much shorter than those of the families themselves, which imposes significant restrictions
178 on the value of the CTM's integration step. For example, the daytime lifetimes of OH and HO_2
179 above 70 km are about 1 s or less, while the lifetime of the HO_x family is about 10^4 s or more.
180 Therefore, when calculating these components individually it is necessary to set the CTM's
181 integration step to be much less than 1 s. In our work, the Shimazaki technique is applied for
182 calculating the evolution of each component of the HO_x and NO_x families. We emphasize that this
183 technique does not explicitly use the steady-state approximation for the components, instead it
184 utilizes the approach based on an implicit Euler scheme (see Shimazaki, 1985). This allows
185 increasing the integration step of CTM significantly without loss of accuracy of calculating the short-
186 lived components. In our work the integration time is chosen to be 9 s.

The model includes 3D advective and vertical diffusive transport (turbulent and molecular). Three-dimensional fields of temperature and winds are taken from the Canadian Middle Atmosphere Model (CMAM) for the year 2000 (de Grandpre et al., 2000; Scinocca et al., 2008). We use the Walcek-scheme (Walcek and Aleksic, 1998; Walcek, 2000) for advective transport and the implicit Thomas algorithm as described in Morton and Mayers (1994) for diffusive transport. The vertical eddy diffusion coefficient is based on the results by Lübken (1997).

The CTM driven by COMMA-IAP middle atmosphere dynamics (Berger, 1994; Ebel et al., 1995; Kremp et al., 1999; Berger and von Zahn, 1999) was verified by measurements, particularly for ozone, in a number of papers (Hartogh et al., 2004, 2011; Sonnemann et al., 2006, 2007).

We calculate the annual variation of spatio-temporal distributions of OH, HO_2, and O_3 and constructed distributions of the $F(OH,HO_2,O_3)$ function introduced in Sect. 1. To remove transitional regions that correspond to sunset and sunrise, we take into account only periods of local time with the solar zenith angle $\chi < 85°$. The obtained results are presented in the model coordinates, so the pressure-height levels are used for the vertical axes. In addition, the approximate altitudes are shown in the figures of Sec. 1, calculated for a given month utilizing averaged temperature profiles of the model and hydrostatic equilibrium.

3. Daytime photochemical equilibrium of OH, HO_2, and O_3 at the altitudes of the mesosphere

The daytime balance of OH concentration at mesospheric altitudes is determined by the following primary reactions (Brasseur and Solomon, 2005):

$HO_2 + O \rightarrow OH + O_2$ (R18 in Table 1)

$H + O_3 \rightarrow OH + O_2$ (R21)

$H + HO_2 \rightarrow 2OH$ (R14)

$OH + O \rightarrow H + O_2$ (R17)

$OH + O_3 \rightarrow HO_2 + O_2$ (R22)

The daytime balance of HO_2 concentration:

$H + O_2 + M \rightarrow HO_2 + M$, M is molecule of air (R20)

$OH + O_3 \rightarrow HO_2 + O_2$ (R22)

$HO_2 + O \rightarrow O_2 + OH$ (R18)

The daytime balance of O_3 concentration:

$O + O_2 + M \rightarrow O_3 + M$ (R12)

$O_3 + h\nu \rightarrow O_2 + O$ (R52)

$O_3 + h\nu \rightarrow O_2 + O(^1D)$ (R53)

$O_3 + H \rightarrow OH + O_2$ (R21)

Expressions for local concentrations of OH, HO_2, and O_3 in the photochemical equilibrium are written in the form

$$OH = \frac{k_{18} \cdot HO_2 \cdot O + 2k_{14} \cdot HO_2 \cdot H + k_{21} \cdot O_3 \cdot H}{k_{17} \cdot O + k_{22} \cdot O_3}, \quad (1)$$

$$HO_2 = \frac{k_{20} \cdot M \cdot O_2 \cdot H + k_{22} \cdot O_3 \cdot OH}{k_{18} \cdot O}, \quad (2)$$

$$O_3 = \frac{k_{12} \cdot M \cdot O_2 \cdot O}{k_{52} + k_{53} + k_{21} \cdot H}, \quad (3)$$

where k_i are the corresponding reaction constants from Burkholder et al. (2015).

We eliminate O and H from Eqs. (1)-(3) and derive an expression depending only on OH, HO_2, O_3.

Almost everywhere in the mesosphere and lower thermosphere (with the exception of 85-95 km, see Kulikov et al., 2017) the photodissociation is the main ozone sink, i.e. $k_{52} + k_{53} >> k_{21} \cdot H$. Therefore, in the zero order approximation Eq. (3) can be simplified and the concentration of atomic oxygen can be defined in terms of ozone concentration:

$$O = \frac{k_{52} + k_{53}}{k_{12} \cdot M \cdot O_2} O_3 \quad (4)$$

Making use of Eq. (4) we can derive from Eq. (2) an expression for the concentration of H in terms of concentrations of OH, HO_2 and O_3:

$$H = \frac{k_{18} \cdot (k_{52} + k_{53}) / (k_{12} \cdot M \cdot O_2) \cdot HO_2 - k_{22} \cdot OH}{k_{20} \cdot M \cdot O_2} O_3 \quad (5)$$

By substituting this equation and Eq. (4) into Eq. (1) we obtain an expression relating OH, HO_2, and O_3:

$$F(OH, HO_2, O_3) = \left(\frac{k_{20} \cdot M \cdot O_2}{k_{20} \cdot M \cdot O_2 + k_{21} \cdot O_3 + 2 \cdot k_{14} \cdot HO_2} + \frac{k_{12} \cdot M \cdot O_2 \cdot k_{22}}{(k_{52} + k_{53}) \cdot k_{17}}\right) \cdot \frac{k_{17} \cdot OH}{k_{18} \cdot HO_2} = 1 \quad (6)$$

Figure 1 shows height–latitude cross-sections of $< F(OH, HO_2, O_3) >$ for each month (in this Section angle brackets denote monthly averaged zonal mean values). The dashed area corresponds to $\chi > 85°$. One can see that eq. (15) is most accurate within the 50–76 km range and

above 86 km, where $|< F > -1| \le 1\%$. The difference reaches 3–4 % in the region between 76 km and 86 km. The altitude of this region has an annual variation with a maximum deviation in the winter hemisphere. Below 50 km the value of $< F >$ increases up to 1.2 at 40 km, thus below the stratopause Eq. (6) no longer describes the simultaneous photochemical equilibrium of OH, HO_2 and O_3. Note that these components remain short-lived below 50 km (with the lifetimes of about 10^2-10^3 s (Brasseur and Solomon, 2005)) depending on height and duration of daylight. However, for quantitative description of their daytime equilibrium it is necessary to include additional reactions involving, in particular, the components of the NO_x family.

Note also that Eq. (1) and Eq. (6) take into account only the main daytime source of OH (P_{OH}) specified by reactions R18, R14, and R21:

$$P_{OH}=k_{18} \cdot HO_2 \cdot O + 2k_{14} \cdot HO_2 \cdot H + k_{21} \cdot O_3 \cdot H$$

These reactions run “inside” the HOx (H, OH, HO_2, H_2O_2) family and do not perturb its total concentration. The height–latitude cross-sections of $< P_{OH} >$ for each month are presented in Fig. 2.

The next important daytime source of OH is specified by reactions R59 and R7 involving H_2O, the main source for the HO_x family:

$$P_{OH}^{H_2O}=(k_{59} + 2 \cdot k_7 \cdot O(^1D)) \cdot H_2O$$

Figure 3 shows height–latitude cross-sections of $< P_{OH}^{H_2O} / P_{OH} >$ for each month. Comparing Fig. 1 and Fig. 3, we conclude that the previously indicated 3–4 % deviation of $< F >$ from 1 in the region between 76 km and 86 km is largely due to the neglect of these reactions.

Another source of OH is sporadically activated during charged particle precipitation events and exists for a relatively short time (several days). Solar proton events (SPE) perturb the ionic composition in the mesosphere and the upper stratosphere considerably and trigger a whole cascade of reactions involving ions, neutral components and their clusters (e.g., $O_2^+ \cdot H_2O$). This leads to an additional (to reactions R59 and R7) conversion of H_2O molecules into OH and H (Solomon et al., 1981). The maximum of the OH production rate (P_{OH}^{SPE}) induced by SPE is located in the polar latitudes in the region of 60–80 km and, as a rule, does not exceed $2 \cdot 10^3$ cm^{-3} s^{-1} (Jackman et al., 2011, 2014). It can be seen from Fig. 2 that at these latitudes and altitudes the P_{OH}^{SPE} / P_{OH} ratio does not exceed 1-2%, even for the maximum values of P_{OH}^{SPE}. This means that

the impact of P_{OH}^{SPE} on Eq. (6) is of the same order of smallness as in the case of reactions R59 and R7, hence, it may be neglected. A similar conclusion can be made for other reactions from Table 1, not accounted for by Eq. (6), including the ones involving NO_x in both quiet and perturbed conditions in the mesosphere.

4. Method of statistical evaluation of simultaneous measurement of OH, HO_2 and O_3

The proposed method is based on the statistical Bayesian procedure described in the works by Kulikov et al. (2009) and Nechaev et al. (2016). It was originally developed for retrieving trace gas concentrations in the mesosphere from ground-based and satellite measurements of other mesospheric components. With respect to the considered evaluation problem this procedure consists of three steps: (1) constructing conditional probability density function (PDF) of OH, HO_2 and O_3 concentration values at each altitude z in the selected interval assuming that there is certain measurement data of these components and the algebraic relationship (6) is valid; (2) calculating the first moments of this distribution, i.e. expected value and dispersion of each component using the Metropolis-Hastings algorithm (Chib and Greenberg, 1995) for multidimensional integration; (3) comparing the obtained results with the initial measurement data.

For constructing posterior PDF it is convenient to introduce vector $\vec{u}\left\{HO_2^{ret}, O_3^{ret}, OH^{ret}\right\}$, whose components are the retrieved values of chemical species concentrations at a certain altitude z, and vector $\vec{x}\left\{HO_2^{m}, O_3^{m}, OH^{m}\right\}$ composed of experimentally measured values of the components of vector $\vec{u}$, $x_j = u_j + \xi_j$, $j = 1..3$, where ξ_j is a random error of measuring the j-th component of vector $\vec{u}$ at the altitude z. It is assumed that

(1) random variables ξ_j are distributed normally with densities

$$w_j(\xi_j) = \frac{1}{\sigma_j\sqrt{2\pi}} exp\left(-\frac{\xi_j^2}{2\sigma_j^2}\right); \quad (7)$$

(2) ξ_j are mutually independent:

$$\vec{\xi}\left\{\xi_1, \xi_2, \xi_3\right\} \sim W_\xi(\vec{\xi}) = \prod_j w_j(\xi_j), \quad (8)$$

where $W_\xi(\vec{\xi})$ is the total PDF of all ξ_j;

299 (3) dispersions σ_j in Eq. (7), that are expected error values, are assumed to be known a priori (in
300 our case they are provided by the MLS retrieval algorithm along with measured data).
301 Then the probability to observe vector $\vec{x}$ is given by the conditional PDF

302 $$P_x(\vec{x}\,|\,\vec{u}) = \int \delta\left(\vec{x}-\vec{u}\right) W_\xi(\vec{\xi}')\, d^3\vec{\xi}' = W_\xi\left(\vec{x}-\vec{u}\right), \qquad (9)$$

303 where $\delta(\ldots)$ is delta function.

304 The prior relationship of HO_2^{ret}, O_3^{ret} and OH^{ret} concentrations (Eq. (6)) can be written as
305 $u_3 = G\left(u_1, u_2\right)$. Integrating the left-hand side of Eq. (17) with conditional PDF of the variable u_3:

306 $$P_{u_3}(u_3\,|\,u_1,u_2) = \delta\left(u_3 - G\left(u_1,u_2\right)\right),$$

307 yields a likelihood function of the model

308 $$P_x(\vec{x}\,|\,u_1,u_2) = w_3\left(x_3 - G\left(u_1,u_2\right)\right)\cdot w_1\left(x_1-u_1\right) w_2\left(x_2-u_2\right). \qquad (10)$$

309 According to Bayes' theorem, the posterior function, i.e. the probability density of latent variables u_1
310 and u_2, under the condition that $\vec{x}$ is observed, is defined by the expression

311 $$\begin{aligned} P(u_1,u_2\,|\,\vec{x}) &\propto P_x(\vec{x}\,|\,u_1,u_2)\cdot P_{apr}\left(u_1,u_2\right) \\ &\propto exp\left(-\frac{\left(x_1-u_1\right)^2}{2\sigma_1^2}\right)\cdot exp\left(-\frac{\left(x_2-u_2\right)^2}{2\sigma_2^2}\right)\cdot exp\left(-\frac{\left(x_3-G\left(u_1,u_2\right)\right)^2}{2\sigma_3^2}\right)\cdot P_{apr}\left(u_1,u_2\right) \end{aligned} \qquad (11)$$

312 in which $P_{apr}\left(u_1,u_2\right)$ defines prior PDF of u_1 and u_2.

313 The retrieved value of the latent variable $u_{1,2,3}$ is hereinafter understood as the mean value
314 of the function in Eq. (11):

315 $$\begin{aligned} \left\langle u_{1,2}\right\rangle &= \int_{-\infty}^{\infty}\int_{-\infty}^{\infty} u_{1,2}\cdot P(u_1,u_2\,|\,\vec{x})\, du_1 du_2 \\ \left\langle u_3\right\rangle &= \int_{-\infty}^{\infty}\int_{-\infty}^{\infty} G\left(u_1,u_2\right)\cdot P(u_1,u_2\,|\,\vec{x})\, du_1 du_2. \end{aligned} \qquad (12)$$

316 Its dispersion defines the uncertainty of the retrieval:

317 $$\sigma_{u_j} = \sqrt{\left\langle u_j^2\right\rangle - \left\langle u_j\right\rangle^2}, \quad j = 1..3, \qquad (13)$$

318 where the angle brackets denote averaging in the sense of Eq. (12).
319
320 **5. MLS/Aura data evaluation and results**

We used the latest version (v4.2) of the MLS "standard" product (Livesey et al., 2017) for trace gas concentrations and temperature T within the 1 – 0.046 mbar pressure interval where all data are suitable for scientific applications (Wang et al., 2015a,b; Schwartz et al., 2015). We took the daytime data when the solar zenith angle $\chi < 80°$ for January, May, and September 2005. All data were appropriately screened. "Pressure", "estimated precision", "status flag", "quality", "convergence" and "clouds" fields were taken into account. HO_2 data were seen as the day-minus-night difference as prescribed by the MLS data guidelines (Livesey et al., 2017). Following Pickett et al. (2008), each daytime profile of this component measured on a given day at a latitude Lat, a profile resulting from averaging the nighttime profiles of HO_2, measured on the same day in the latitude range of Lat±5°, was subtracted. This operation eliminates systematic biases affecting HO_2 retrievals, but limits the studied latitude range to the one where MLS observes both daytime and nighttime data.

The integrals in Eq. (12)–(13) were calculated at every pressure level p for each set of simultaneously measured vertical profiles $OH^{MLS}(p)$, $HO_2^{MLS}(p)$, $O_3^{MLS}(p)$, $T^{MLS}(p)$, $\sigma_{OH^{MLS}}(p)$, $\sigma_{HO_2^{MLS}}(p)$, $\sigma_{O_3^{MLS}}(p)$. The vertical profiles $<OH^{ret}>(p)$, $<HO_2^{ret}>(p)$, $<O_3^{ret}>(p)$, $\sigma_{OH^{ret}}(p)$, $\sigma_{HO_2^{ret}}(p)$, $\sigma_{O_3^{ret}}(p)$ were found at each point of the globe along the satellite track. Numerical integration was performed by a Monte Carlo method. For each pressure level, a sample of about $5 \cdot 10^5$ pairs of random variable values $\{u_1, u_2\} = \{HO_2^{ret}, O_3^{ret}\}$ distributed with normalized probability density given by Eq. (11) with $P_{apr}(u_1, u_2) \equiv 1$ was generated with the help of the Metropolis-Hastings algorithm (Chib and Greenberg, 1995). In this case, the statistical moments in Eq. (12)–(13) were determined by summation over the sample.

A typical example of retrieved profiles HO_2^{ret}, O_3^{ret} and OH^{ret} (black curves) in comparison with the measured HO_2^{MLS}, O_3^{MLS} and OH^{MLS} (red curves) is given in Fig. 4. First of all, note that statistics of the retrieved data is in satisfactory agreement with the initial measurement of OH and O_3 concentrations, but not of HO_2. The error of satellite measurement, $\sigma_{HO_2^{MLS}}$, greatly exceeds the uncertainty of retrieval, $\sigma_{HO_2^{ret}}$, so at some altitudes the values of $<HO_2^{MLS}>$ (red dashed curves) do not fall within the corresponding intervals $<HO_2^{ret}> \pm \sigma_{HO_2^{ret}}$. Second, the results of a single

measurement of all three components and their retrieved values have considerable uncertainties relative to their means within the whole interval of altitudes. Therefore, the observed and retrieved data should be compared using the commonly accepted approach (e.g., Pickett et al., 2008) of averaging large ensembles of profiles within certain latitude and time ranges, or zones. It is supposed that the noise of satellite measurement instruments is delta-correlated, so that random values corresponding to each single measured or retrieved profile are statistically independent. In this case the dispersion of a measured or retrieved zonal mean profile is determined by summation

$$\sigma^2{}_{\Sigma} = \frac{1}{N^2}\sum_{k=1}^{N}\sigma^2{}_k ,$$

where N is the number of measured or retrieved profiles within the zone and $\sigma^2{}_k$ is the dispersion of the k-th measured or retrieved profile.

The range of latitudes covered by the satellite trajectory was divided into 17 bins 10^0 each. About 3000 single profiles of each chemical component fall into one bin during a month of MLS/Aura observations. Therefore, the resulting uncertainties due to measurement noise of OH, HO_2 and O_3 concentration profiles (both measured and retrieved) averaged over such ensembles are significantly (about one and a half order of magnitude) lower than the uncertainties of individual profiles. Examples of such profiles for January, May and September 2005 are presented in Fig. 5. One can see that the indicated uncertainties are now small enough to make clear conclusions about the extent to which the observed and retrieved profiles agree by comparing their averaged values only, i.e. $<OH^{MLS}>$, $<HO_2{}^{MLS}>$, $<O_3{}^{MLS}>$ and $<OH^{ret}>$, $<HO_2{}^{ret}>$, $<O_3{}^{ret}>$.

Figures 4–6 show monthly averaged zonal mean pressure–latitude cross-sections of $<HO_2{}^{ret}>$, $<HO_2{}^{MLS}>$, $\Delta HO_2 = (<HO_2{}^{ret}> - <HO_2{}^{MLS}>)/<HO_2{}^{MLS}>$ and similar characteristics for OH and O_3 concentration profiles for three months of the year 2005. First, clearly, the distributions of $<OH^{ret}>$ and $<O_3{}^{ret}>$ are in good qualitative and quantitative agreement with the initial MLS/Aura measurement data at lower altitudes, below ~ 0.07 mbar and 0.1 mbar, correspondingly. At higher altitudes, the distributions of $<OH^{ret}>$ reproduce all the main structural features of $<OH^{MLS}>$, but the retrieved OH concentration has lower values than the observed one with a relative difference ΔOH reaching ~15% at the top. The distribution of $<O_3{}^{ret}>$ above 0.1 mbar, in turn, differs considerably from $<O_3{}^{MLS}>$, both in quantity and quality, and ΔO_3 locally

reaches 50-60% and more. Second, for all months there are significant qualitative and quantitative differences between $<HO_2^{ret}>$ and $<HO_2^{MLS}>$, the most noticeable one being location of the mesospheric maximum of this component's concentration. According to the observations it is close to 0.1 mbar, while the retrieved data demonstrate the altitudes of about ~0.046 mbar or higher. Our analysis of the applied method of statistical evaluation demonstrates that the higher position of this maximum in the distributions of $<HO_2^{ret}>$ is influenced by the OH^{MLS} data in which the mesospheric maximum (see Figs. 6-8) is also located notably higher than 0.1 mbar.

6. Discussion and conclusion

On the basis of the data presented in Section 5 we can conclude that, upon the whole, simultaneous OH, HO_2 and O_3 satellite measurements poorly satisfy the photochemical equilibrium condition. The HO_2 component biases from this condition most prominently. We can conjecture that a possible explanation for the bias is the significant systematic error in HO_2 measurements, in particular, in the height of the mesospheric maximum. This assumption is supported by the calculation of the HO_2 distributions with the use of our 3D chemical transport model (see Fig. 9). It can be seen that the mesospheric maximum of HO_2 in these months, as well as of the $<HO_2^{ret}>$ distributions, lies above 0.046 mbar.

Moreover, new data on the HO_2 distributions were recently obtained from the MLS measurements. Millán et al. (2015) performed the offline retrieval of daily zonal means of HO_2 profiles using averaged MLS radiances measured in 10° latitude bins. Averaged spectra have a better signal to noise ratio, which removes many of the limitations of the MLS standard product for HO_2. In particular, the upper boundary of the altitude region in which daytime data is suitable for scientific use has reached 0.0032 mbar, and the "day-minus-night" correction is not needed at altitudes above 1 mbar. Comparison with various experimental and model data has shown that the offline retrieval reproduces the basic properties of the HO_2 distribution in the mesosphere relatively well (at least qualitatively) (Millán et al. 2015).

The offline retrieval product, the alternative dataset of daytime HO_2, has recently become publicly available at https://mls.jpl.nasa.gov. Figure 10 shows the monthly averaged zonal means of offline retrieval data ($<HO_2^{MLS}{}_{offline}>$) and relative differences with retrieved and MLS standard

product data $(<HO_2^{MLS}> - <HO_2^{MLS}_{offline}>)/ <HO_2^{MLS}_{offline}>$ and $(<HO_2^{ret}> - <HO_2^{MLS}_{offline}>)/ <HO_2^{MLS}_{offline}>$, correspondingly. Figure 10 represents the same time periods as Figs. 6-8. It is worth noting that the distributions $<HO_2^{MLS}_{offline}>$ depicted in Fig. 10 represent significantly different amounts of data. The data sets for May and September include 31 and 27 days of measurements, respectively, whereas the January dataset encompasses only 4 days. The latter makes the graphs in the first row in Fig. 10 noisier than the others. One can see that the results of the offline HO_2 retrieval show the same features as the results of our evaluation technique in comparison to the standard MLS retrieval, i.e. the height of mesospheric HO_2 maximum is notably higher. We can conclude that the distributions of $<HO_2^{ret}>$ better match $<HO_2^{MLS}_{offline}>$ than $<HO_2^{MLS}>$, although some quantitative discrepancy between $<HO_2^{ret}>$ and $<HO_2^{MLS}_{offline}>$ also exists. Note that this may be due to systematic errors in the HO_2^{MLS} distributions, which cannot be excluded within the framework of the introduced technique. For a detailed qualitative and quantitative comparison of $<HO_2^{ret}>$ and $<HO_2^{MLS}_{offline}>$ one should modify the method, so that a statistical evaluation of the OH^{MLS} and O_3^{MLS} standard products, and the data of the offline HO_2 retrieval could be conducted within the framework of a single procedure with no account for the HO_2^{MLS} distributions. This modification is under way and will be presented elsewhere.

The proposed method for statistical evaluation of mesospheric species measurements can be readily generalized to other atmospheric photochemical systems that contain short-lived components (see Introduction). It may also be modified for assessing hard to measure chemical components, characteristics of atmospheric processes (like wind speed or turbulent diffusion rate), or poorly known reaction rates.

Acknowledgments

This work was supported by the Russian Science Foundation (contract No. 15–17–10024 of June 04, 2015). The data used in this study is supported by the Institute of Applied Physics of the Russian Academy of Sciences (Nizhny Novgorod, Russia). Inquiries about the distributions used in this paper can be addressed to Mr. Belikovich (belikovich@ipfran.ru).

References

Avallone, L. M., and Toohey, D. W.: Tests of halogen photochemistry using in situ measurements of ClO and BrO in the lower polar stratosphere, J. Geophys. Res., Volume 106, Issue D10, Pages 10411–1042, doi: 10.1029/2000JD900831, 2001.

Benton, A. K., Langridge, J. M., Ball, S. M., Bloss, W. J., Dall'Osto, M., Nemitz, E., Harrison, R. M., and Jones, R. L.: Night-time chemistry above London: measurements of NO3 and N2O5 from the BT Tower, Atmos. Chem. Phys., 10, 9781-9795, doi:10.5194/acp-10-9781-2010, 2010.

Berger, U.: Numerische Simulation klimatologischer Prozesse und thermische Gezeiten in der mittleren Atmosph¨are, Thesis, Univ. Cologne, Germany, 1994.

Berger, U. and von Zahn, U.: The two-level structure of the mesopause: A model study, J. Geophys. Res., 104, 22083–22093, 1999.

Berthet, G., Ricaud, P., Lefevre, F., Le Flochmoen, E., Urban, J., Barret, B., Lautie, N., Dupuy, E., De La Noe, J., and Murtagh, D.: Nighttime chlorine monoxide observations by the Odin satellite and implications for the ClO/Cl_2O_2 equilibrium, Geophys. Res. Lett., 32, L11812, doi:10.1029/2005GL022649, 2005.

Brasseur, G. and Solomon, S.: Aeronomy of the Middle Atmosphere, 644 pp., 3rd edition, Springer, The Netherlands, 2005.

Brown, S. S., Stark, H., Ryerson, T. B., Williams, E. J., Nicks Jr., D. K., Trainer, M., Fehsenfeld, F. C., and Ravishankara, A. R.: Nitrogen oxides in the nocturnal boundary layer: Simultaneous in situ measurements of NO_3, N_2O_5, NO_2, NO, and O_3, J. Geophys. Res., 108(D9), 4299, doi:10.1029/2002JD002917, 2003.

Burkholder, J. B., S. P. Sander, J. Abbatt, J. R. Barker, R. E. Huie, C. E. Kolb, M. J. Kurylo, V. L. Orkin, D. M. Wilmouth, and P. H. Wine (2015), Chemical Kinetics and Photochemical Data for Use in Atmospheric Studies, Evaluation No. 18, JPL Publication 15-10, Jet Propulsion Laboratory, Pasadena, http://jpldataeval.jpl.nasa.gov.

Butz, A., H. Bosch, C. Camy-Peyret, M. Dorf, A. Engel, S. Payan, and Pfeilsticker, K.: Observational constraints on the kinetics of the ClO-BrO and ClO-ClO ozone loss cycles in the Arcticwinter stratosphere, Geophys. Res. Lett., 34, L05801, doi:10.1029/2006GL028718, 2007.

Cantrell, C. A., Mauldin, L., Zondlo, M., Eisele, F., Kosciuch, E., Shetter, R., Lefer, B., Hall, S., Campos, T., Ridley, B., Walega, J., Fried, A., Wert, B., Flocke, F., Weinheimer, A., Hannigan,

J., Coffey, M., Atlas, E., Stephens, S., Heikes, B., Snow, J., Blake, D., Blake, N., Katzenstein, A., Lopez, J., Browell, E. V., Dibb, J., Scheuer, E., Seid, G., and Talbot, R.: Steady state free radical budgets and ozone photochemistry during TOPSE, J. Geophys. Res., 108(D4), 8361, doi:10.1029/2002JD002198, 2003.

Chameides, W.: Tropospheric odd nitrogen and the atmospheric water vapor cycle, J. Geophys. Res., 84 (C10), 4989–4996, doi: 10.1029/JC080i036p04989, 1975.

Chib, S., and Greenberg, E.: Understanding the Metropolis-Hastings Algorithm, The American Statistician, 49 (4), 327-335, doi: 10.2307/2684568, 1995.

Crawford, J., Davis, D., Chen, G., Bradshaw, J., Sandholm, S., Gregory, G., Sachse, G., Anderson, B., Collins, J., Blake, D., Singh, H., Heikes, B., Talbot, R., Rodriguez, J.: Photostationary state analysis of the NO_2-NO system based on airborne observations from the western and central North Pacific, 101(D1), 2053–2072, doi: 10.1029/95JD02201, 1996.

Crowley, J. N., Schuster, G., Pouvesle, N., Parchatka, U., Fischer, H., Bonn, B., Bingemer, H., and Lelieveld, J.: Nocturnal nitrogen oxides at a rural mountain-site in south-western Germany, Atmos. Chem. Phys., 10, 2795-2812, doi:10.5194/acp-10-2795-2010, 2010.

de Grandpre, J., Beagley, S. R., Fomichev, V. I., Griffioen, E., McConnell, J. C., Medvedev, A. S., and Shepherd., T. G.: Ozone climatology using interactive chemistry: Results from the Canadian Middle Atmosphere Model, J. Geophys. Res.-Atmos., 105, 26475-26491, doi:10.1029/2000JD900427, 2000.

Djouad, R., Michelangeli, D. V., and Gong, W.: Numerical solution for atmospheric multiphase models: Testing the validity of equilibrium assumptions, J. Geophys. Res., 108(D19), 4602, doi:10.1029/2002JD002969, 2003.

Douglass, A. R., Jackman, C. H., and Stolarski, R. S.: Comparison of model results transporting the odd nitrogen family with results transporting separate odd nitrogen species, J. Geophys. Res., 94(D7), 9862–9872, doi:10.1029/JD094iD07p09862, 1989.

Ebel, A., Berger, U., and Krueger, B. C.: Numerical simulations with COMMA, a global model of the middle atmosphere, SIMPO Newsletter, 12, 22–32, 1995.

Evans, W. F. J., and Llewellyn, E. J.: Atomic hydrogen concentrations in the mesosphere and the hydroxyl emissions, J. Geophys. Res., 78, 323–326, doi:10.1029/JA078i001p00323, 1973.

Evans, W.F.J., McDade, I. C., Yuen, J., and Llewellyn, E. J.: A rocket measurement of the O_2 infrared atmospheric (0-0) band emission in the dayglow and a determination of the

mesospheric ozone and atomic oxygen densities, Can. J. Phys., 66, 941–946, doi:10.1139/p88-15, 1988.

Feigin, A. M., and Konovalov, I. B.: On the possibility of complicated dynamic behavior of atmospheric photochemical systems: Instability of the Antarctic photochemistry during the ozone hole formation, J. Geophys. Res., 101, 26023–26038, doi:10.1029/96JD02011, 1996.

Feigin, A. M., Konovalov, I. B., and Molkov, Ya. I.: Towards understanding nonlinear nature of atmospheric photochemistry: Essential dynamic model of the mesospheric photochemical system, J. Geophys. Res., 103, 25447–25460, doi:10.1029/98JD01569, 1998.

Funke, B., Lopez-Puertas, M., von Clarmann, T., Stiller, G. P., Fischer, H., Glatthor, N., Grabowski, U., Hopfner, M., Kellmann, S., Kiefer, M., Linden, A., Mengistu Tsidu, G., Milz, M., Steck, T. and Wang, D. Y.: Retrieval of stratospheric NOx from 5.3 and 6.2 mm nonlocal thermodynamic equilibrium emissions measured by Michelson Interferometer for Passive Atmospheric Sounding (MIPAS) on Envisat, J. Geophys. Res., 110, D09302, doi:10.1029/2004JD005225, 2005.

Ghosh, S., Pyle, J. A., and Good, P.: Temperature dependence of the ClO concentration near the stratopause, J. Geophys. Res., 102(D15), 19207–19216, doi:10.1029/97JD01099, 1997.

Good, R. E.: Determination of atomic oxygen density from rocket borne measurements of hydroxyl airglow, Planet. Space Sci., 24, 389–395, doi.org/10.1016/0032-0633(76)90052-0, 1976.

Grygalashvyly, M., Sonnemann, G. R., and Hartogh, P.: Long-term behavior of the concentration of the minor constituents in the mesosphere—A model study, Atmos. Chem. Phys., 9, 2779–2792, doi:10.5194/acp-9-2779-2009, 2009.

Grygalashvyly, M., Becker, E., and Sonnemann, G. R.: Wave mixing effects on minor chemical constituents in the MLT region: Results from a global CTM driven by high-resolution dynamics, J. Geophys. Res., 116, D18302, doi:10.1029/2010JD015518, 2011.

Grygalashvyly, M., Becker, E., and Sonnemann, G. R.: Gravity wave mixing and effective diffusivity for minor chemical constituents in the mesosphere/lower thermosphere, Space Sci. Rev., 168, 333–362, doi:10.1007/s11214-011-9857-x, 2012.

Grygalashvyly, M., Sonnemann, G. R., Lübken, F.-J., Hartogh, P., and Berger, U.: Hydroxyl layer: Mean state and trends at midlatitudes, J. Geophys. Res.-Atmos., 119, 12391–12419, doi:10.1002/2014JD022094, 2014.

Grygalashvyly, M.: Several notes on the OH* layer, Ann. Geophys., 33, 923-930, doi:10.5194/angeo-33-923-2015, 2015.

Hartogh, P., Jarchow, C., Sonnemann, G. R., and Grygalashvyly, M.: On the spatiotemporal behavior of ozone within the upper mesosphere/mesopause region under nearly polar night conditions, J. Geophys. Res., 109, D18303, doi:10.1029/2004JD004576, 2004.

Hartogh, P., Sonnemann, G. R., Grygalashvyly, M., and Jarchow, Ch.: Ozone trends in mid-latitude stratopause region based on microwave measurements at Lindau (51.66° N, 10.13° E), the ozone reference model, and model calculations, Adv. Space Res., 47, 1937-1948, doi:10.1016/j.asr.2011.01.010, 2011.

Hauchecorne, A., Bertaux, J. L., Dalaudier, F., Keckhut, P., Lemennais, P., Bekki, S., Marchand, M., Lebrun, J. C., Kyrölä, E., Tamminen, J., Sofieva, V., Fussen, D., Vanhellemont, F., Fanton d'Andon, O., Barrot, G., Blanot, L., Fehr, T., and Saavedra de Miguel, L.: Response of tropical stratospheric O_3, NO_2 and NO_3 to the equatorial Quasi-Biennial Oscillation and to temperature as seen from GOMOS/ENVISAT, Atmos. Chem. Phys., 10, 8873-8879, doi:10.5194/acp-10-8873-2010, 2010.

Jackman, C. H., Marsh, D. R., Vitt, F. M., Roble, R. G., Randall, C. E., Bernath, P. F., Funke, B., López-Puertas, M., Versick, S., Stiller, G. P., Tylka, A. J., and Fleming, E. L.: Northern Hemisphere atmospheric influence of the solar proton events and ground level enhancement in January 2005, Atmos. Chem. Phys., 11, 6153-6166, https://doi.org/10.5194/acp-11-6153-2011, 2011.

Jackman, C. H., Randall, C. E., Harvey, V. L., Wang, S., Fleming, E. L., López-Puertas, M., Funke, B., and Bernath, P. F.: Middle atmospheric changes caused by the January and March 2012 solar proton events, Atmos. Chem. Phys., 14, 1025-1038, https://doi.org/10.5194/acp-14-1025-2014, 2014.

Kawa, S. R., Fahey, D. W., Solomon, S., Brune, W. H., Proffitt, M. H., Toohey, D. W., Anderson Jr., D. E., Anderson, L. C., and Chan, K. R.: Interpretation of aircraft measurements of NO, ClO, and O_3 in the lower stratosphere, J. Geophys. Res., 95(D11), 18597–18609 doi: 10.1029/JD095iD11p18597, 1990.

Kremp, C., Berger, U., Hoffmann, P., Keuer, D., and Sonnemann, G. R.: Seasonal variation of middle latitude wind fields of the mesopause region – a comparison between observation and model calculation, Geophys. Res. Lett., 26, 1279–1282, 1999.

559 Kaye, J. A., and Rood, R. B.: Chemistry and transport in a three-dimensional stratospheric
560 model: Chlorine species during a simulated stratospheric warming, J. Geophys. Res., 94(D1),
561 1057–1083, doi: 10.1029/JD094iD01p01057, 1989.
562 Ko, M., Hu, W., Rodriguez, J. M., Kondo, Y., Koike, M., Kita, K., Kawakami, S., Blake, D.,
563 Liu, S., and Ogawa, T.: Photochemical ozone budget during the BIBLE A and B campaigns, J.
564 Geophys. Res., 107, 8404, doi:10.1029/2001JD000800, 2002. [printed 108(D3), 2003].
565 Kondo, Y., Matthews, W. A., Aimedieu, P., and Robbins, D. E. Diurnal variation of nitric
566 oxide at 32 km: Measurements and interpretation, J. Geophys. Res., 93(D3), 2451–2460,
567 doi:10.1029/JD093iD03p02451, 1988.
568 Kondo, Y., Ziereis, H., Koike, M., Kawakami, S., Gregory, G. L., Sachse, G. W., Singh, H.
569 B., Davis, D. D., Merrill, J. T.: Reactive nitrogen over the Pacific Ocean during PEM-West, A
570 101(D1), 1809–1828, doi:10.1029/95JD02611, 1996.
571 Konovalov, I. B., Feigin, A. M., Mukhina, A. Y.: Toward understanding of the nonlinear
572 nature of atmospheric photochemistry: Multiple equilibrium states in the high-latitude lower
573 stratospheric photochemical system, J. Geophys. Res, 104, 8669-8689,
574 doi:10.1029/1998JD100037, 1999.
575 Konovalov, I. B., and Feigin, A. M.: Toward an understanding of the nonlinear nature of
576 atmospheric photochemistry: Origin of the complicated dynamic behaviour of the mesospheric
577 photochemical system, Nonlin. Processes Geophys., 7, 87–104, doi:10.5194/npg-7-87-2000, 2000.
578 Körner, U., and Sonnemann, G. R.: Global 3D-modeling of water vapor concentration of the
579 mesosphere/mesopause region and implications with respect to the NLC region, J. Geophys. Res.-
580 Atmos., 106, 9639– 9651, doi:10.1029/2000JD900744, 2001.
581 Kowalewski, S., von Savigny, C., Palm, M., McDade, I. C., and Notholt, J.: On the impact of
582 the temporal variability of the collisional quenching process on the mesospheric OH emission layer:
583 a study based on SD-WACCM4 and SABER, Atmos. Chem. Phys., 14, 10193-10210,
584 doi:10.5194/acp-14-10193-2014, 2014.
585 Kremser, S., Schofield, R., Bodeker, G. E., Connor, B. J., Rex, M., Barret, J., Mooney, T.,
586 Salawitch, R. J., Canty, T., Frieler, K., Chipperfield, M. P., Langematz, U., and Feng, W.: Retrievals
587 of chlorine chemistry kinetic parameters from Antarctic ClO microwave radiometer measurements,
588 Atmos. Chem. Phys., 11, 5183-5193, doi:10.5194/acp-11-5183-2011, 2011.

Kulikov, M. Y., Feigin, A. M., and Sonnemann, G. R.: Retrieval of the vertical distribution of chemical components in the mesosphere from simultaneous measurements of ozone and hydroxyl distributions, Radiophys. Quantum Electron., 49, 683–691, doi:10.1007/s11141-006-0103-4, 2006.

Kulikov, M. Yu., Feigin, A. M., and Sonnemann, G. R.: Retrieval of water vapor profile in the mesosphere from satellite ozone and hydroxyl measurements by the basic dynamic model of mesospheric photochemical system, Atmos. Chem. Phys., 9, 8199-8210, doi:10.5194/acp-9-8199-2009, 2009.

Kulikov, M. Y., Mukhin, D. N., and Feigin, A. M.: Bayesian strategy of accuracy estimation for characteristics retrieved from experimental data using base dynamic models of atmospheric photochemical systems, Radiophys. Quantum Electron., 52, 618–626, doi:10.1007/s11141-010-9171-6, 2009.

Kulikov, M. Yu., Vadimova, O. L., Ignatov, S. K., and Feigin, A.M.: The mechanism of non-linear photochemical oscillations in the mesopause region, Nonlinear Processes in Geophysics, v.19, p.p.501–512, doi:10.5194/npg-19-501-2012, 2012.

Kulikov, M. Yu., and Feigin, A. M.: Automated construction of the basic dynamic models of the atmospheric photochemical systems using the RADM2 chemical mechanism as an example, Radiophys. Quantum Electron., 57, 478-487, doi 10.1007/s11141-014-9530-9, 2014.

Kulikov, M. Y., Belikovich, M. V., Grygalashvyly, M., Sonnemann, G. R., Ermakova, T. S., Nechaev, A. A., and Feigin, A. M.: Daytime ozone loss term in the mesopause region, Ann. Geophys., 35, 677-682, doi:10.5194/angeo-35-677-2017, 2017.

Livesey, N. J., Read, W. G., Wagner, P. A., Frovideaux, L., Lambert, A., Manney, G. L., Millan, L. F., Pumphrey, H. C., Santee, M. L., Schwartz, M. J., Wang, S., Fuller, R. A., Jarnot, R. F., Knosp, B. W., and Martinez E.: Earth Observing System (EOS) Aura Microwave Limb Sounder (MLS) Version 4.2 Level 2 data quality and description document, JPL D-33509, JPL publication, USA, 2017.

Llewellyn, E. J., McDade, I. C., Moorhouse, P., and Lockerbie, M. D.: Possible reference models for atomic oxygen in the terrestrial atmosphere, Adv. Space Res., 13, 135–144, doi:0.1016/0273-1177(93)90013-2, 1993.

Llewellyn, E. J., and McDade, I. C.: A reference model for atomic oxygen in the terrestrial atmosphere, Adv. Space Res., 18, 209–226, doi:10.1016/0273-1177(96)00059-2, 1996.

Lubken, F. J.: Seasonal variation of turbulent energy dissipation rates at high latitudes as determined by in situ measurements of neutral density fluctuations, J. Geophys. Res., 102, 13441–13456, 1997.

Marchand, M., Bekki, S., Lefevre, F., and Hauchecorne, A.: Temperature retrieval from stratospheric O3 and NO3 GOMOS data, Geophys. Res. Lett., 34, L24809, doi:10.1029/2007GL030280, 2007.

Marsh, D. R., Smith, A. K., Mlynczak, M. G., and Russell III, J. M.: SABER observations of the OH Meinel airglow variability near the mesopause, J. Geophys. Res., 111, A10S05, doi:10.1029/2005JA011451, 2006.

Martinez, M., Perner, D., Hackenthal, E.-M., Kulzer, S., and Schultz, L.: NO_3 at Helgoland during the NORDEX campaign in October 1996, J. Geophys. Res., 105(D18), 22,685–22,695, doi:10.1029/2000JD900255, 2000.

Massie, S. T., and Hunten, D. M.: Stratospheric eddy diffusion coefficients from tracer data, J. Geophys. Res., 86(C10), 9859–9868, doi:10.1029/JC086iC10p09859, 1981.

McDade, I. C., Llewellyn, E. J., and Harris, F. R.: Atomic oxygen concentrations in the lower auroral thermosphere, Adv. Space Res., 5(7), 229–232, doi:10.1016/0273-1177(85)90379-5, 1985.

McDade, I. C., and Llewellyn, E. J.: Mesospheric oxygen atom densities inferred from night-time OH Meinel band emission rates, Planet. Space Sci., 36, 897–905, DOI:10.1016/0032-0633(88)90097-9, 1988.

McLaren, R., Wojtal, P., Majonis, D., McCourt, J., Halla, J. D., and Brook, J.: NO_3 radical measurements in a polluted marine environment: links to ozone formation, Atmos. Chem. Phys., 10, 4187-4206, doi:10.5194/acp-10-4187-2010, 2010.

Millán, L., Wang, S., Livesey, N., Kinnison, D., Sagawa, H., and Kasai, Y.: Stratospheric and mesospheric HO_2 observations from the Aura Microwave Limb Sounder, Atmos. Chem. Phys., 15, 2889-2902, doi:10.5194/acp-15-2889-2015, 2015.

Mlynczak, M. G., and Solomon, S.: Middle atmosphere heating by exothermic chemical reactions involving odd-hydrogen species, Geophys. Res. Lett., 18, 37-40, doi:10.1029/90GL02672, 1991.

Mlynczak, M. G., and Solomon, S.: A detailed evaluation of the heating efficiency in the middle atmosphere, J. Geophys. Res., 98, 10,517–10,541, doi:10.1029/93JD00315, 1993.

649 Mlynczak, M. G., Marshall, B. T., Martin-Torres, F. J., Russell III, J. M., Thompson, R. E.,
650 Remsberg, E. E., and Gordley, L. L.: Sounding of the Atmosphere using Broadband Emission
651 Radiometry observations of daytime mesospheric O2(1D) 1.27 μm emission and derivation of
652 ozone, atomic oxygen, and solar and chemical energy deposition rates, J. Geophys. Res., 112,
653 D15306, doi:10.1029/2006JD008355, 2007.
654 Mlynczak, M. G., Hunt, L. A., Mast, J. C., Marshall, B. T., Russell III, J. M., Smith, A. K.,
655 Siskind, D. E., Yee, J.-H., Mertens, C. J., Martin-Torres, F. J., Thompson, R. E., Drob, D. P., and
656 Gordley, L. L.: Atomic oxygen in the mesosphere and lower thermosphere derived from SABER:
657 Algorithm theoretical basis and measurement uncertainty, J. Geophys. Res., 118, 5724–5735,
658 doi:10.1002/jgrd.50401, 2013a.
659 Mlynczak, M. G., Hunt, L. H., Mertens, C. J., Marshall, B. T., Russell III, J. M., López-
660 Puertas, M., Smith, A. K., Siskind, D. E., Mast, J. C., Thompson, R. E., and Gordley, L. L.:
661 Radiative and energetic constraints on the global annual mean atomic oxygen concentration in the
662 mesopause region, J. Geophys. Res. Atmos., 118, 5796–5802, doi:10.1002/jgrd.50400, 2013b.
663 Mlynczak, M. G., Hunt, L. A., Marshall, B. T., Mertens, C. J., Marsh, D. R., Smith, A. K.,
664 Russell, J. M., Siskind, D. E., and Gordley, L. L.: Atomic hydrogen in the mesopause region
665 derived from SABER: Algorithm theoretical basis, measurement uncertainty, and results, J.
666 Geophys. Res., 119, 3516–3526, doi:10.1002/2013JD021263, 2014.
667 Morton, K. W., and D. F. Mayers, Numerical Solution of Partial Differential Equations,
668 Cambridge University Press, 1994.
669 Nechaev, A. A., Ermakova, T. S., and Kulikov, M. Y.: Determination of the Trace-Gas
670 Concentrations at the Altitudes of the Lower and Middle Mesosphere from the Time Series of
671 Ozone Concentration, Radiophys. Quantum Electron., 59, 546–559, doi:10.1007/s11141-016-
672 9722-6, 2016.
673 Nikoukar, R., Swenson, G. R., Liu, A. Z., and Kamalabadi, F.: On the variability of
674 mesospheric OH emission profiles, J. Geophys. Res., 112, D19109, doi:10.1029/2007JD008601,
675 2007.
676 Pendleton, W. R., Baker, K. D., and Howlett, L. C.: Rocket-based investigations of $O(^3P)$,
677 $O_2(a^1\Delta_g)$ and OH*($\nu=1,2$) during the solar eclipse of 26 February1979, J. Atm. Terr. Phys., 45 (7),
678 479 – 491, doi:10.1016/S0021-9169(83)81108-8, 1983.

679 Penkett, S. A., Monks, P. S., Carpenter, L. J., Clemitshaw, K. C., Ayers, G. P., Gillett, R. W.,
680 Galbally, I. E., and Meyer, C. P.: Relationships between ozone photolysis rates and peroxy radical
681 concentrations in clean marine air over the Southern Ocean, J. Geophys. Res., 102(D11), 12805–
682 12817, doi:10.1029/97JD00765, 1997.
683 Penkett, S. A., Reeves, C. E., Bandy, B. J., Kent, J. M., and Richer, H. R.: Comparison of
684 calculated and measured peroxide data collected in marine air to investigate prominent features of
685 the annual cycle of ozone in the troposphere, J. Geophys. Res., 103(D11), 13377–13388,
686 doi:10.1029/97JD02852, 1998.
687 Platt, U., Perner, D., and Pätz, H. W.: Simultaneous measurement of atmospheric CH2O,
688 O3, and NO2 by differential optical absorption, J. Geophys. Res., 84(C10), 6329–6335,
689 10.1029/JC084iC10p06329, 1979.
690 Pyle, J. A., Zavody, A. M., Harries, J. E., and Moffat, P. H.: Derivation of OH concentration
691 from satellite infrared measurements of NO_2 and HNO_3, Nature, 305, 690-692,
692 doi:10.1038/305690a0, 1983.
693 Pyle, J. A., and Zavody, A. M.: The derivation of hydrogen containing radical concentrations
694 from satellite data sets, Q. J. R. Meteorol. Soc., 111, 993-1012, doi:10.1002/qj.49711147005,
695 1985.
696 Pickett, H. M., and Peterson, D. B.: Comparison of measured stratospheric OH with
697 prediction, J. Geophys. Res., 101(D11), 16789–16796, doi: 10.1029/96JD01168, 1996.
698 Pickett, H. M., Drouin, B. J., Canty, T., Salawitch, R. J., Fuller, R. A., Perun, V. S., Livesey,
699 N. J., Waters, J. W., Stachnik, R. A., Sander, S. P., Traub, W. A., Jucks, K. W., and Minschwaner,
700 K.: Validation of Aura Microwave Limb Sounder OH and HO2 measurements, J. Geophys. Res.,
701 113, D16S30, doi:10.1029/2007JD008775, 2008.
702 Rasch, P. J., Boville, B. A., and Brasseur, G. P.: A three-dimensional general circulation
703 model with coupled chemistry for the middle atmosphere, J. Geophys. Res., 100(D5), 9041–9071,
704 doi: 10.1029/95JD00019, 1995.
705 Russell, J. P., and Lowe, R. P.: Atomic oxygen profiles (80–94 km) derived from Wind
706 Imaging Interferometer/Upper Atmospheric Research Satellite measurements of the hydroxyl
707 airglow: 1. Validation of technique, J. Geophys. Res., 108, 4662, doi:10.1029/2003JD003454, D21,
708 2003.

Schwartz, M., Froidevaux, L., Livesey, N., and Read, W.: MLS/Aura Level 2 Ozone (O_3) Mixing Ratio V004, Greenbelt, MD, USA, Goddard Earth Sciences Data and Information Services Center (GES DISC), accessed 13.07.16, doi:10.5067/AURA/MLS/DATA2017, 2015.

Scinocca, J. F., McFarlane, N. A., Lazare, M., Li, J., Plummer, D.: The CCCma third generation AGCM and its extension into the middle atmosphere, Atmos. Chem. Phys., 8, 7055-7074, doi:10.5194/acp-8-7055-2008, 2008.

Shimazaki, T.: Minor Constituents in the Middle Atmosphere, D. Reidel, Norwell, Mass., USA, 444 pp., 1985.

Siskind, D. E., Marsh, D. R., Mlynczak, M. G., Martin-Torres, F. J., and Russell III, J. M.: Decreases in atomic hydrogen over the summer pole: Evidence for dehydration from polar mesospheric clouds?, Geophys. Res. Lett., 35, L13809, doi:10.1029/2008GL033742, 2008.

Siskind D. E., Mlynczak, M. G., Marshall, T., Friedrich, M., Gumbel, J.: Implications of odd oxygen observations by the TIMED/SABER instrument for lower D region ionospheric modeling, J. Atmos. Sol. Terr. Phys., 124, 63–70, doi: 10.1016/j.jastp.2015.01.014, 2015.

Smith, A. K., Marsh, D. R., Mlynczak, M. G., and Mast, J. C.: Temporal variations of atomic oxygen in the upper mesosphere from SABER, J. Geophys. Res., 115, D18309, doi:10.1029/2009JD013434, 2010.

Sobanski, N., Tang, M. J., Thieser, J., Schuster, G., Pöhler, D., Fischer, H., Song, W., Sauvage, C., Williams, J., Fachinger, J., Berkes, F., Hoor, P., Platt, U., Lelieveld, J., and Crowley, J. N.: Chemical and meteorological influences on the lifetime of NO3 at a semi-rural mountain site during PARADE, Atmos. Chem. Phys., 16, 4867-4883, doi:10.5194/acp-16-4867-2016, 2016.

Solomon, S., Rusch, D. W., Gerard, J.-C., Reid, G. C., and Crutzen, P. J.: The effect of particle precipitation events on the neutral and ion chemistry of the middle atmosphere. 2. Odd hydrogen, Planet. Space Sci., 29, 885–892, 1981.

Sonnemann, G., Kremp, C., Ebel, A., and Berger, U.: A three-dimensional dynamic model of minor constituents of the mesosphere, Atmos. Environ., 32, 3157–3172, doi:10.1016/S1352-2310(98)00113-7, 1998.

Sonnemann, G. R., Grygalashvyly, M., Hartogh, P., and Jarchow, C.: Behavior of mesospheric ozone under nearly polar night conditions, Adv. Space Res., 38, 2402–2407, doi:10.1016/j.asr.2006.09.011, 2006.

Sonnemann, G. R., Hartogh, P., Jarchow, C., Grygalashvyly, M., and Berger, U.: On the winter anomaly of the night-to-day ratio of ozone in the middle to upper mesosphere in middle to high latitudes, Adv. Space Res., 40, 846–854, doi:10.1016/j.asr.2007.01.039, 2007.

Sonnemann, G. R., Hartogh, P., Berger, U., and Grygalashvyly, M.: Hydroxyl layer: trend of number density and intra-annual variability Ann. Geophys., 33, 749–767, doi:10.5194/angeo-33-749-2015, 2015.

Swenson, G. R., and Gardner, C. S.: Analytical models for the responses of the mesospheric OH* and Na layers to atmospheric gravity waves, J. Geophys. Res., 103(D6), 6271–6294, doi:10.1029/97JD02985, 1998.

Solomon, P., Connor, B., Barrett, J., Mooney, T., Lee, A., and Parrish, A.: Measurements of stratospheric ClO over Antarctica in 1996–2000 and implications for ClO dimer chemistry, Geophys. Res. Lett., 29(15), 1708, doi:10.1029/2002GL015232, 2002.

Stedman, D. H., Chameides, W., and Jackson, J. O.: Comparison of experimental and computed values for J(NO_2), Geophys. Res. Lett., 2(1), 22-25, doi:1029/GL002i001p00022, 1975.

Stimpfle, R. M., Wilmouth, D. M., Salawitch, R. J., and Anderson, J. G.: First measurements of ClOOCl in the stratosphere: The coupling of ClOOCl and ClO in the Arctic polar vortex, J. Geophys. Res., 109, D03301, doi:10.1029/2003JD003811, 2004.

Sumińska-Ebersoldt, O., Lehmann, R., Wegner, T., Grooß, J.-U., Hösen, E., Weigel, R., Frey, W., Griessbach, S., Mitev, V., Emde, C., Volk, C. M., Borrmann, S., Rex, M., Stroh, F., and von Hobe, M.: ClOOCl photolysis at high solar zenith angles: analysis of the RECONCILE self-match flight, Atmos. Chem. Phys., 12, 1353-1365, doi:10.5194/acp-12-1353-2012, 2012.

Thomas, R. J.: Atomic hydrogen and atomic oxygen density in the mesosphere region: Global and seasonal variations deduced from Solar Mesosphere Explorer near-infrared emissions, J. Geophys. Res., 95, 16,457–16,476, doi:10.1029/JD095iD10p16457, 1990.

Tulet, P., Grini, A., Griffin, R. J., and Petitcol, S.: ORILAM-SOA: A computationally efficient model for predicting secondary organic aerosols in three-dimensional atmospheric models, J. Geophys. Res., 111, D23208, doi:10.1029/2006JD007152, 2006.

von Hobe, M., Grooß, J.-U., Müller, R., Hrechanyy, S., Winkler, U., and Stroh, F.: A re-evaluation of the ClO/Cl2O2 equilibrium constant based on stratospheric in-situ observations, Atmos. Chem. Phys., 5, 693-702, doi:10.5194/acp-5-693-2005, 2005.

von Hobe, M., Salawitch, R. J., Canty, T., Keller-Rudek, H., Moortgat, G. K., Grooß, J.-U., Müller, R., and Stroh, F.: Understanding the kinetics of the ClO dimer cycle, Atmos. Chem. Phys., 7, 3055-3069, doi:10.5194/acp-7-3055-2007, 2007.

Walcek, C. J., and N. M. Aleksic (1998), A simple but accurate mass conservative, peak preserving, mixing ratio bounded advection algorithm with Fortran code, Atmos. Environm., 32, 3863-3880.

Walcek, C. J. (2000), Minor flux adjustment near mixing ratio extremes for simplified yet highly accurate monotonic calculation of tracer advection, J. Geophys. Res., 105, 9335-9348.

Wang, S., Pickett, H., Livesey, N., and Read, W.: MLS/Aura Level 2 Hydroperoxy (HO_2) Mixing Ratio V004, Greenbelt, MD, USA, Goddard Earth Sciences Data and Information Services Center (GES DISC), accessed 13.07.16, doi:10.5067/AURA/MLS/DATA2013, 2015a.

Wang, S., Livesey, N., and Read, W.: MLS/Aura Level 2 Hydroxyl (OH) Mixing Ratio V004, Greenbelt, MD, USA, Goddard Earth Sciences Data and Information Services Center (GES DISC), accessed 13.07.16, doi:10.5067/AURA/MLS/DATA2018, 2015b.

Webster, C. R., May, R. D., Toumi, R., and Pyle, J. A.: Active nitrogen partitioning and the nighttime formation of N2O5 in the stratosphere: Simultaneous in situ measurements of NO, NO_2, HNO_3, O_3, and N_2O using the BLISS diode laser spectrometer, J. Geophys. Res., 95(D9), 13851–13866 doi: 10.1029/JD095iD09p13851, 1990.

Wetzel, G., Oelhaf, H., Kirner, O., Friedl-Vallon, F., Ruhnke, R., Ebersoldt, A., Kleinert, A., Maucher, G., Nordmeyer, H., and Orphal, J.: Diurnal variations of reactive chlorine and nitrogen oxides observed by MIPAS-B inside the January 2010 Arctic vortex, Atmos. Chem. Phys., 12, 6581-6592, doi:10.5194/acp-12-6581-2012, 2012.

Xu, J., Smith, A. K., Jiang, G., Gao, H., Wei, Y., Mlynczak, M. G. ,and Russell III, J. M.: Strong longitudinal variations in the OH nightglow, Geophys. Res. Lett., 37, L21801, doi:10.1029/2010GL043972, 2010.

Xu, J., Gao, H., Smith, A. K., and Zhu, Y.: Using TIMED/SABER nightglow observations to investigate hydroxyl emission mechanisms in the mesopause region, J. Geophys. Res., 117, D02301, doi:10.1029/2011JD016342, 2012.

Table 1. List of reactions with corresponding reaction rates from Burkholder et al. (2015).

1	$O(^1D)+O_2 \rightarrow O+O_2$	22	$OH+O_3 \rightarrow O_2+HO_2$	43	$NO_2+O_3 \rightarrow NO_3+O_2$
2	$O(^1D)+N_2 \rightarrow O+N_2$	23	$HO_2+O_3 \rightarrow OH+2O_2$	44	$N+OH \rightarrow NO+H$
3	$O(^1D)+O_3 \rightarrow O_2+2O$	24	$H+OH+N_2 \rightarrow H_2O+N_2$	45	$NO+HO_2 \rightarrow NO_2+OH$
4	$O(^1D)+O_3 \rightarrow 2O_2$	25	$OH+H_2 \rightarrow H_2O+H$	46	$H+NO_2 \rightarrow OH+NO$
5	$O(^1D)+N_2O \rightarrow 2NO$	26	$OH+OH \rightarrow H_2O+O$	47	$NO_3+NO \rightarrow 2NO_2$
6	$O(^1D)+N_2O \rightarrow N_2+O_2$	27	$OH+OH+M \rightarrow H_2O_2+M$	48	$N+NO \rightarrow N_2+O$
7	$O(^1D)+H_2O \rightarrow 2OH$	28	$OH+HO_2 \rightarrow H_2O+O_2$	49	$N+NO2 \rightarrow N2O+O$
8	$O(^1D)+H_2 \rightarrow H+OH$	29	$H_2O_2+OH \rightarrow H_2O+HO_2$	50	$O_2+h\nu \rightarrow 2O$
9	$O(^1D)+CH_4 \rightarrow CH_3+OH$	30	$HO_2+HO_2 \rightarrow H_2O_2+O_2$	51	$O_2+h\nu \rightarrow O+O(^1D)$
10	$O(^1D)+CH_4 \rightarrow H_2+CH_2O$	31	$HO_2+HO_2+M \rightarrow H_2O_2+O_2+M$	52	$O_3+h\nu \rightarrow O_2+O$
11	$O+O+M \rightarrow O_2+M$	32	$CH_3+O \rightarrow CH_2O+H$	53	$O_3+h\nu \rightarrow O_2+O(^1D)$
12	$O+O_2+M \rightarrow O_3+M$	33	$OH+CO \rightarrow H+CO_2$	54	$N_2+h\nu \rightarrow 2N$
13	$O+O_3 \rightarrow O_2+O_2$	34	$CH_4+OH \rightarrow CH_3+H_2O$	55	$NO+h\nu \rightarrow N+O$
14	$H+HO_2 \rightarrow 2OH$	35	$CH_3+O_2+M \rightarrow CH_3O_2+M$	56	$NO_2+h\nu \rightarrow NO+O$
15	$H+HO_2 \rightarrow H_2O+O$	36	$O_3+N \rightarrow NO+O_2$	57	$N_2O+h\nu \rightarrow N_2+O(^1D)$
15	$H+HO_2 \rightarrow H_2+O_2$	37	$NO_3+O \rightarrow NO_2+O_2$	58	$N_2O+h\nu \rightarrow N+NO$
17	$OH+O \rightarrow H+O_2$	38	$O+NO+M \rightarrow NO_2+M$	59	$H_2O+h\nu \rightarrow H+OH$
18	$HO_2+O \rightarrow OH+O_2$	39	$NO_2+O \rightarrow NO+O_2$	60	$CH_4+h\nu \rightarrow CH_2+H_2$
19	$H_2O_2+O \rightarrow OH+HO_2$	40	$NO_2+O+M \rightarrow NO_3+M$	61	$H_2O_2+h\nu \rightarrow 2OH$
20	$H+O_2+M \rightarrow HO_2+M$	41	$N+O_2 \rightarrow NO+O$	62	$NO_3+h\nu \rightarrow NO_2+O$
21	$H+O_3 \rightarrow OH+O_2$	42	$NO+O_3 \rightarrow NO_2+O_2$	63	$CO_2+h\nu \rightarrow CO+O$

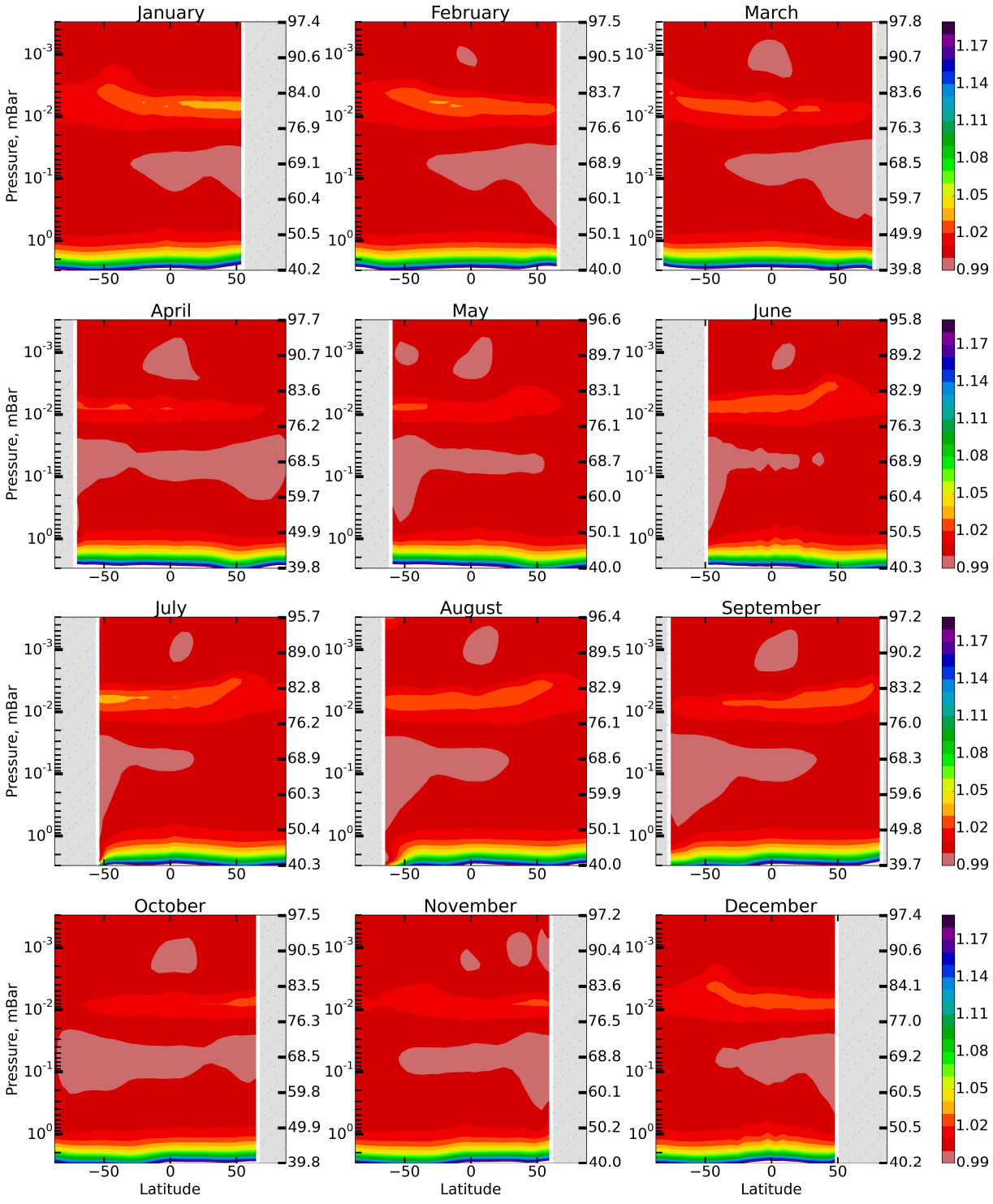

Figure 1. Daytime monthly averaged zonal mean F distributions.

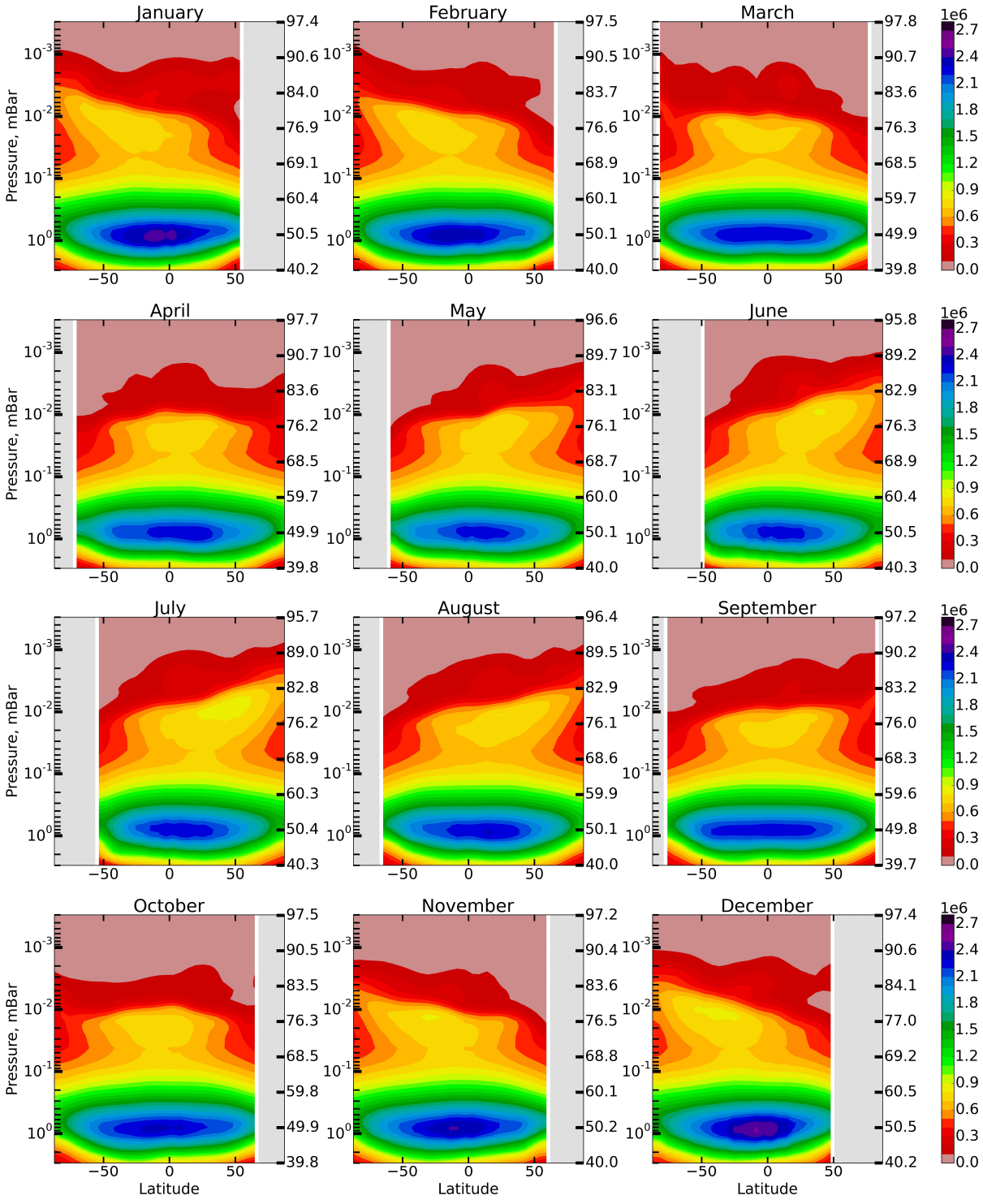

Figure 2. Daytime monthly averaged zonal mean P_{OH} distributions (in $cm^{-3}s^{-1}$).

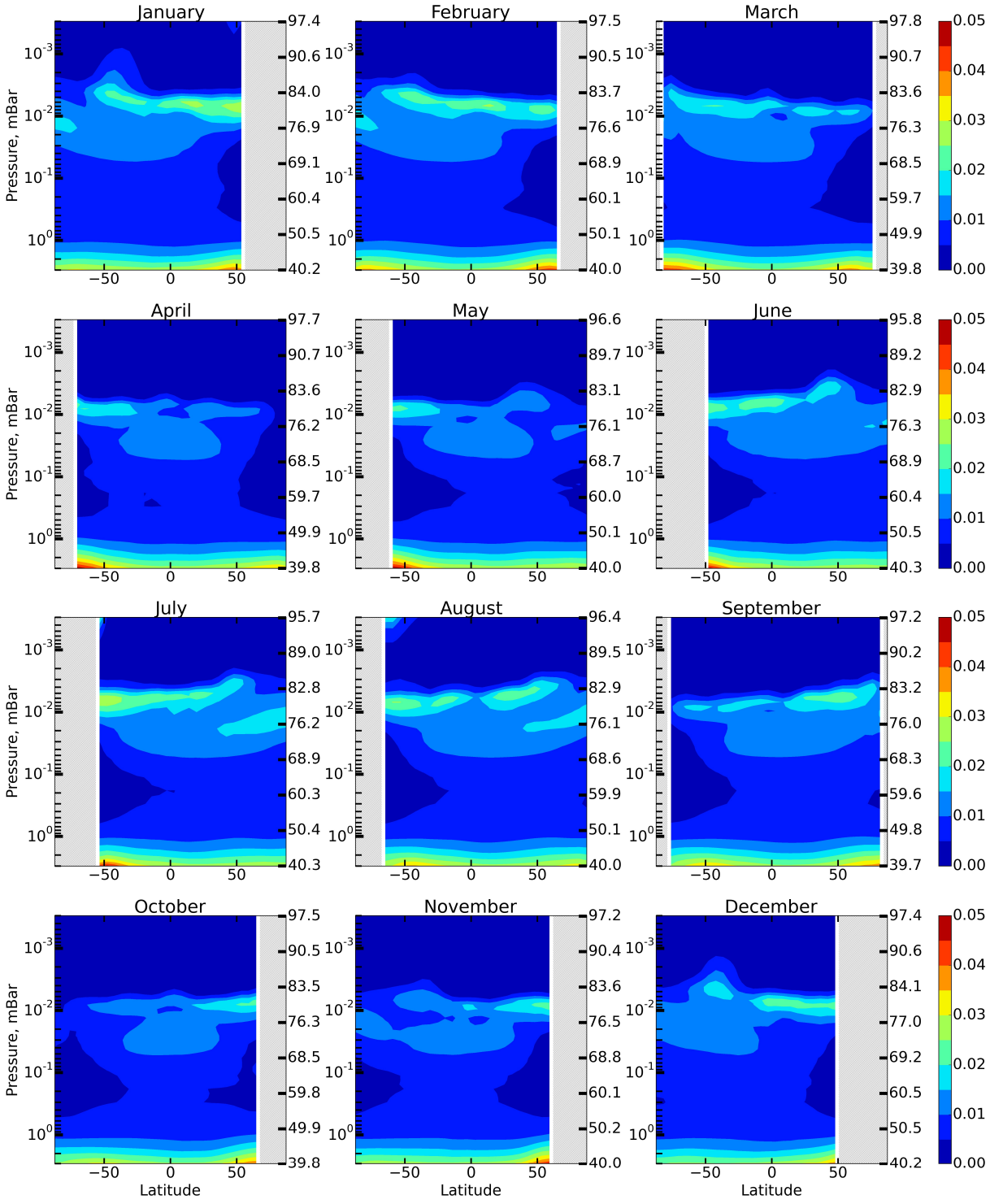

Figure 3. Daytime monthly averaged zonal mean $P_{OH}^{H_2O} / P_{OH}$ distributions.

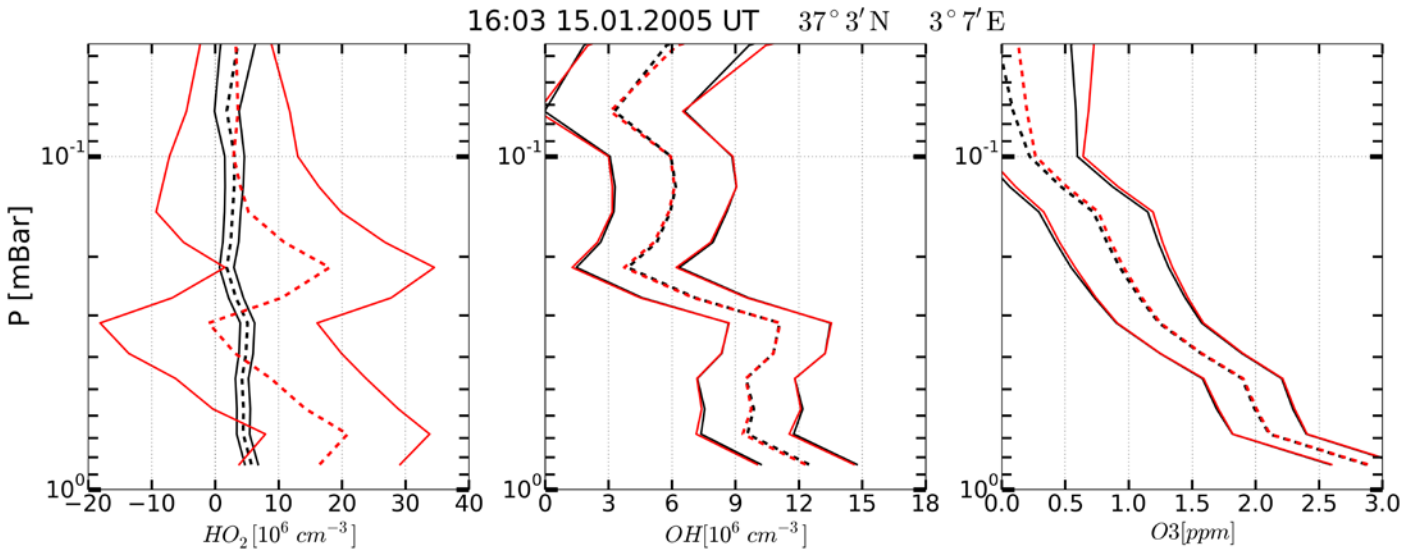

Figure 4. Example of OH, HO_2 and O_3 vertical profiles measured (red curves) on 15 January 2005 at 16.03 UT, $37^0 3'$N, $3^0 7'$E and corresponding retrieved profiles (black curves). Solid curves: boundaries of the 65% confident intervals, dashed curves: medians.

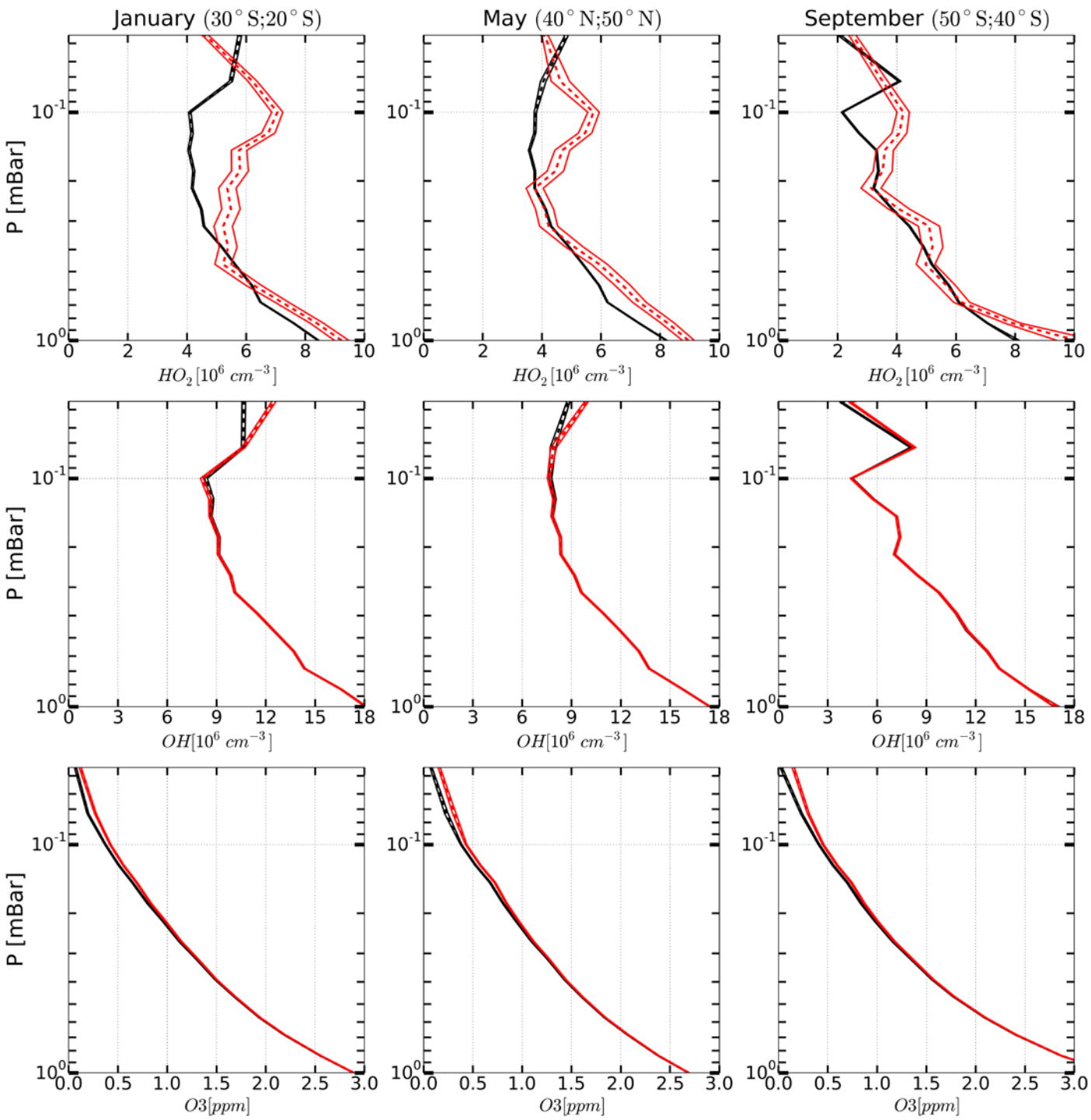

Figure 5. Examples of monthly averaged zonal mean vertical profiles of OH, HO_2 and O_3 measured (red curves) in January, May and March 2005 and corresponding retrieved profiles (black curves). Solid curves: boundaries of the 65% confident intervals, dashed curves: medians.

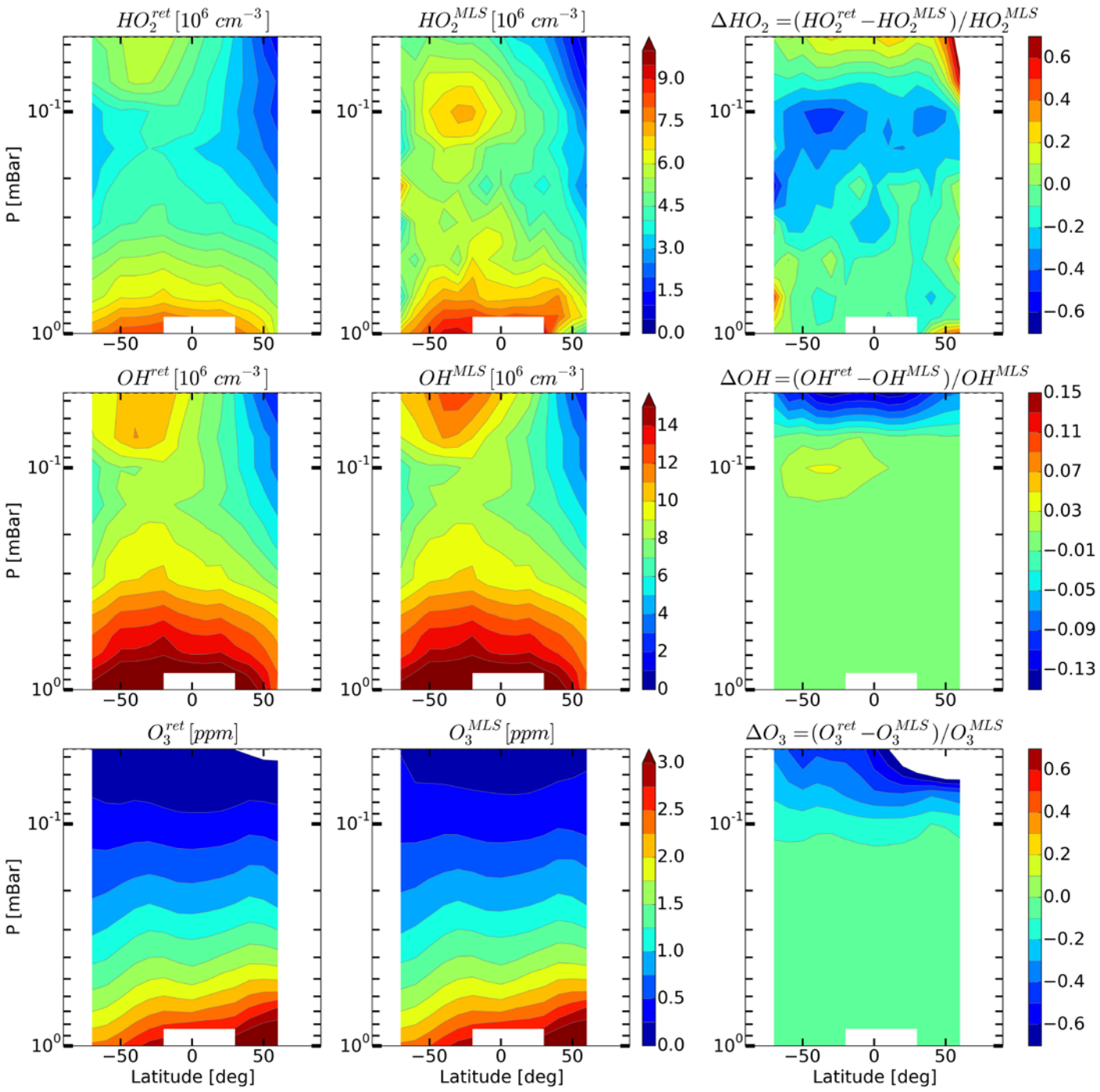

Figure 6. Daytime monthly averaged zonal mean retrieved (left column) and measured (middle column) distributions of HO_2, OH, and O_3 and their relative difference (right column) in January 2005.

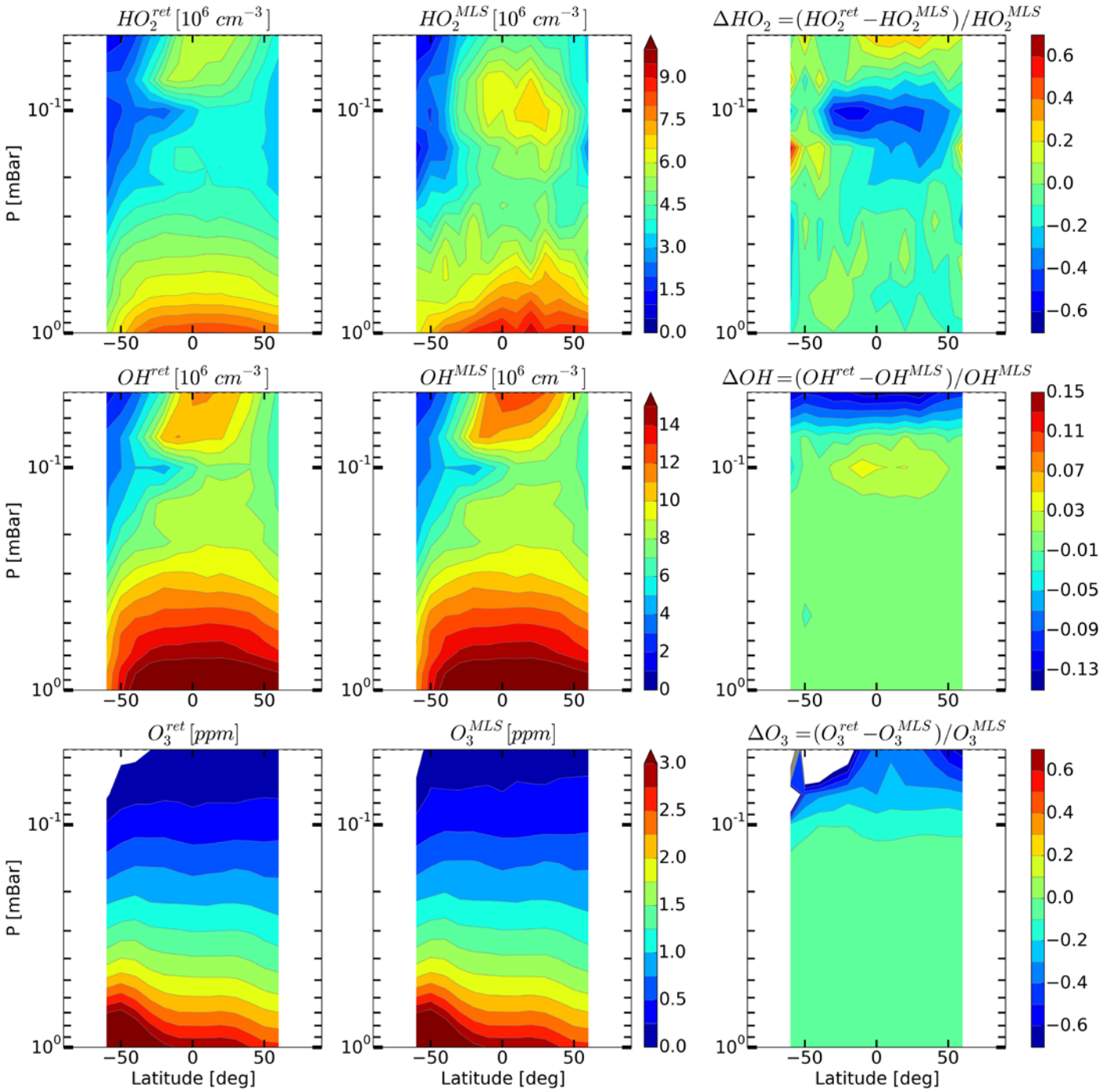

Figure 7. Daytime monthly averaged zonal mean retrieved (left column) and measured (middle column) distributions of HO_2, OH, and O_3 and their relative difference (right column) for May 2005.

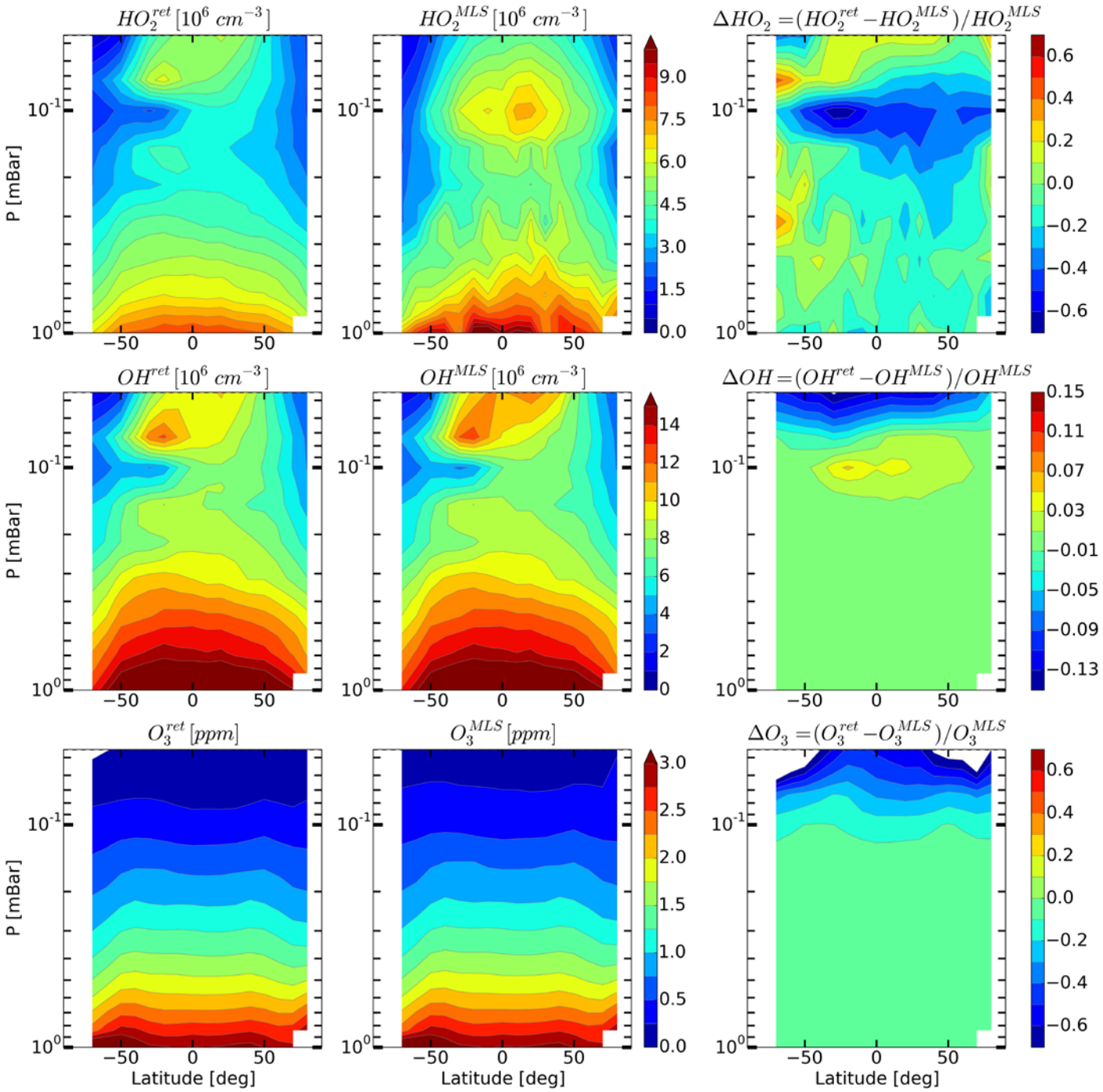

Figure 8. Daytime monthly averaged zonal mean retrieved (left column) and measured (middle column) distributions of HO_2, OH, and O_3 and their relative difference (right column) for September 2005.

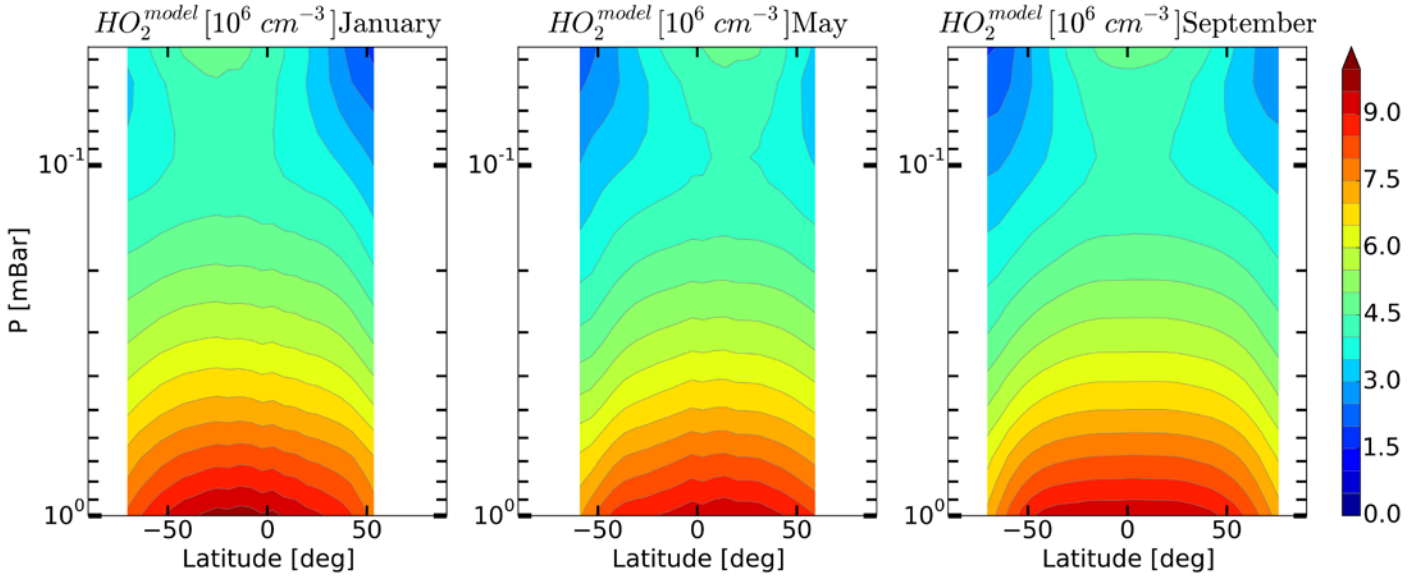

Figure 9. Daytime monthly averaged zonal mean model distributions of HO_2 for January, May, and September.

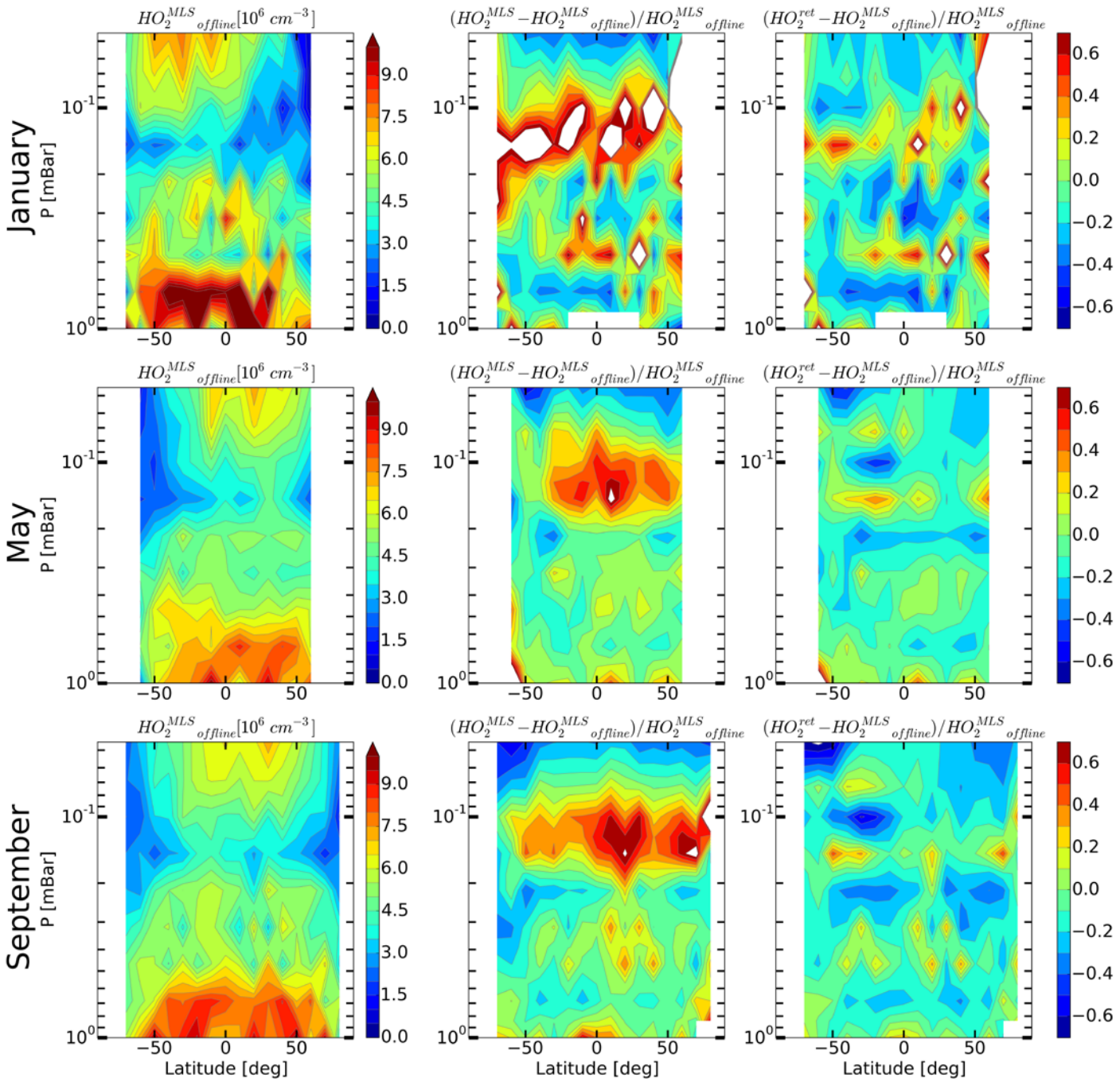

Figure 10. Daytime mean monthly averaged distributions of HO_2 retrieved by Millán et al. (2015) and relative differences $(<HO_2^{MLS}> - <HO_2^{MLS}{}_{offline}>)/<HO_2^{MLS}{}_{offline}>$ and $(<HO_2^{ret}> - <HO_2^{MLS}{}_{offline}>)/<HO_2^{MLS}{}_{offline}>$.